ARNOLD'S MECHANISM OF DIFFUSION IN THE SPATIAL CIRCULAR RESTRICTED THREE-BODY PROBLEM: A SEMI-ANALYTICAL ARGUMENT

AMADEU DELSHAMS[†,♯] , MARIAN GIDEA[‡] AND PABLO ROLDAN[†,§]

Abstract. We consider the spatial circular restricted three-body problem, on the motion of an infinitesimal body under the gravity of Sun and Earth. This can be described by a 3-degree of freedom Hamiltonian system. We fix an energy level close to that of the collinear libration point L_1, located between Sun and Earth. Near L_1 there exists a normally hyperbolic invariant manifold, diffeomorphic to a 3-sphere. For an orbit confined to this 3-sphere, the amplitude of the motion relative to the ecliptic (the plane of the orbits of Sun and Earth) can vary only slightly.

We show that we can obtain new orbits whose amplitude of motion relative to the ecliptic changes significantly, by following orbits of the flow restricted to the 3-sphere alternatively with homoclinic orbits that turn around the Earth. We provide an abstract theorem for the existence of such 'diffusing' orbits, and numerical evidence that the premises of the theorem are satisfied in the three-body problem considered here. We provide an explicit construction of diffusing orbits.

The geometric mechanism underlying this construction is reminiscent of the Arnold diffusion problem for Hamiltonian systems. Our argument, however, does not involve transition chains of tori as in the classical example of Arnold. We exploit mostly the 'outer dynamics' along homoclinic orbits, and use very little information on the 'inner dynamics' restricted to the 3-sphere.

As a possible application to astrodynamics, diffusing orbits as above can be used to design low cost maneuvers to change the inclination of an orbit of a satellite near L_1 from a nearly-planar orbit to a tilted orbit with respect to the ecliptic. We explore different energy levels, and estimate the largest orbital inclination that can be achieved through our construction.

1. Introduction

1. The instability problem in Hamiltonian dynamics. Many physical systems that conserve mechanical energy can be modeled as (autonomous) Hamiltonian systems. Typical Hamiltonian systems exhibit chaotic dynamics. Integrable Hamiltonian systems – those that can be solved by quadratures – are rare. In applications, one

1991 *Mathematics Subject Classification.* Primary, 37J40; 37C50; 37C29; Secondary, 37B30.

Key words and phrases. Three-body problem; Arnold Diffusion; Invariant manifolds; Topological shadowing lemma.

† Research of A.D. and P.R. was partially supported by Spanish MINECO-FEDER Grants MTM2012-31714, MTM2015-65715-P, and Catalan Grant 2014SGR504.

♯ A.D. was also partially supported by the Russian Scientific Foundation Grant 14-41-00044 at the Lobachevsky University of Nizhny Novgorod.

‡ Research of M.G. was partially supported by NSF grants: DMS-0601016 and DMS-1515851.

§ P.R. wants to acknowledge the partial support given by the Asociación Mexicana de Cultura A.C.

frequently encounters *nearly integrable Hamiltonian systems*, which are small perturbations of integrable ones. Studying the long-term behavior of nearly integrable Hamiltonian systems was considered by Poincaré to be *the fundamental problem of dynamics*.

An underlying question is whether the effect of small perturbations averages out in the long run, or it can accumulate to large effects. Arnold [1] conjectured that, for 'typical' nearly-integrable systems, there always exist orbits that *'diffuse'*, i.e., they travel a large distance in the phase space, for all sufficiently small perturbations. A brief overview on Arnold's diffusion problem and on recent progress is given in subsection 6 below. Many results on the Arnold diffusion problem concern 'generic' classes of Hamiltonian systems. There are only few concrete examples in the literature where diffusing orbits can be found explicitly.

2. Model and main results. In this paper we describe a simple model from celestial mechanics which exhibits diffusing orbits.

We also describe a general method, relying on geometric and topological tools, that can be used to find explicitly such orbits. This method can be applied to other models not considered in this paper (see. e.g. [7]).

We consider the spatial circular restricted three-body problem (SCRTBP), in the case of the Sun-Earth system. This models the motion of an infinitesimal particle (satellite) relative to two massive bodies (Sun and Earth), which are assumed to move on circular orbits about their center of mass. In the spatial problem the infinitesimal particle is not constrained to move in the same plane as the massive bodies (the ecliptic plane).

This system can be described by a 3-degree of freedom Hamiltonian system. There are five equilibrium points for the Hamiltonian flow: three of them are of center-center-saddle type, and the other two are of center-center-center type. In this paper we focus on one of the center-center-saddle equilibria, referred to as L_1, which is located between Sun and Earth. (We point out that we can carry a similar analysis on the other two equilibria of center-center-saddle type.)

The dynamics near L_1 is organized by some remarkable geometric objects. For an energy level close to that of L_1, the flow restricted to the energy manifold has a 3-dimensional normally hyperbolic invariant manifold (NHIM) near L_1.

The NHIM is diffeomorphic to a 3-sphere, and contains many 2-dimensional invariant tori that are closely spaced. (The existence of families of 2-dimensional invariant tori as above can be established, under certain restrictions on the parameters of the model, by using the KAM theorem.) Thus, any orbit of the *'inner dynamics'* — the restriction of the flow to the 3-sphere — is either confined to an invariant torus, or to one of the narrow *'gaps'* between two invariant 2-tori that separate the 3-sphere. For each orbit lying on such a torus the out-of plane amplitude relative to the ecliptic is fixed, and for each orbit lying inside a gap the out-of plane amplitude varies only very little. Thus, there are no orbits for the inner dynamics that can 'diffuse' across the sphere; in other words, it it is impossible to achieve a large change of the out-of-plane amplitude of an orbit by using only the inner dynamics. In this sense, the inner dynamics is similar to that of an integrable system.

In order to obtain orbits that diffuse across the sphere one has to use also the *'outer dynamics'* – along homoclinic orbits bi-asymptotic to the 3-sphere. As it

turns out, the stable and unstable manifolds of the 3-sphere intersect transversally, yielding multiple homoclinic manifolds, which consist of smooth families of homoclinic orbits. By following carefully selected homoclinic orbits one can increase/decrease the out-of-plane amplitude by an amount that is larger than the size of the gaps between the invariant tori. We construct pseudo-orbits — obtained by repeatedly intertwining the outer dynamics with the inner dynamics — that *change the out-of-plane amplitude by a 'large amount'*. We then show, via a *topological version of the shadowing lemma*, that there exist true orbits that follow closely those pseudo-orbits.

Our methodology combines analytical results with numerical methods. The main analytical result is an abstract theorem that provides the existence of diffusing orbits under verifiable conditions. The numerical part consists of verifying the conditions of the theorem, and of explicitly detecting diffusing orbits through careful computations. More details are given in subsection 4 below.

3. Applications. A possible application of this mechanism is to design low cost procedures that change the out-of-plane amplitude, relative to the ecliptic, of the motion of a satellite near L_1, from nearly zero amplitude to some 'large' amplitude. We also provide practical information on how to choose the energy level of the system in order to obtain such motions that end up near the largest possible out-of-plane amplitude for that energy level.

Our focus on L_1 can be viewed as a 'proof of concept'. Similar type of orbits can be designed near the other equilibrium points of center-center-saddle type.

We also point out that in this paper we consider a relatively narrow range of energies near that of L_1. At higher energies, new types of orbits appear – the so called halo orbits –, which are rather useful for space mission design. In practice, it is not too difficult to jump to the halo orbits (see [36]). At higher energies, the dynamics restricted to the 3-sphere does no longer resemble that of an nearly-integrable system – the Poincaré section reveals large 'elliptic islands' and a large 'stochastic sea'. Hence, the underlying dynamics is not nearly integrable, as in the case of the Arnold diffusion problem, which is one of the motivations of our work. In fact, the closer the energy level is to that of L_1, the closer the dynamics on the 3-sphere is to that of an integrable system, hence the more difficult is to achieve diffusion. So in this paper we deliberately choose to consider a more difficult problem.

4. Methodology. In his original paper [1], Arnold described a mechanism of diffusion based on transition chains consisting of KAM tori and transverse heteroclinic connections among them. Such transition chains were also used in other papers, e.g., [48, 26, 18, 54, 16, 20, 9]. Other mechanisms of diffusion make use of transition chains of secondary tori [16], or of Aubry-Mather sets [11, 12, 31].

In comparison to the works mentioned above, in this paper we do not use transition chains formed by invariant tori or by Aubry Mather sets. Instead, we parametrize the 3-sphere near L_1 by a system of coordinates consisting of one action and two angle variables, – with the action variable corresponding to the out-of-plane amplitude of the orbit about the ecliptic –, and form transition chains of level sets of the action. These level sets are not necessarily invariant sets, but only 'almost invariant'. Once we obtain a parametrization of the 3-sphere by action-angle variables, computing level sets of the action is trivial. Consequently, our method is

computationally very cheap. In contrast, the precise computation of KAM tori, secondary tori, or Aubry-Mather sets is more laborious.

We mention that transition chains of level sets of the action also appear in [32], but they have not been numerically implemented before.

Now we briefly explain the construction of transition chains of action level sets. The main tool is a geometrically defined mapping on the NHIM, referred to as the scattering map (see [21]). For a fixed choice of a homoclinic manifold, follow an unstable fiber whose foot point lies on the NHIM up to the homoclinic manifold; then identify a stable fiber that passes through the same homoclinic point, and follow the stable fiber up to its foot point on the NHIM; the mapping that assigns to the foot point of the unstable fiber the foot point of the stable fiber is the scattering map. In order for this map to be well defined, one has to fix a suitable restriction of the homoclinic manifold. The resulting scattering map is in general defined only on some open subset of the NHIM.

The scattering map provides a convenient way to track the effect on the action variable of following homoclinic orbits. Applying the scattering map to a level set of the action variable yields points that lie on higher levels of the action variable, as well as points that lie on lower levels of the action variable. In order to achieve a consistent effect of the scattering map on successive action level sets — say, to keep increasing the value of the action — one has first to select those locations where the scattering map goes from a lower action level to a higher action level. Then, after applying the scattering map, one has to move along the action level set in order to reach out a location where another application of the scattering map increases again the value of the action variable. That is, one has to intersperse successive applications of the scattering maps with conveniently long trajectories of the dynamics restricted to the 3-sphere. In our model, a homoclinic excursion – corresponding to one application of the scattering map – is represented by a trajectory that starts near L_1, makes a turn around the Earth, and returns close to L_1, and an orbit of the inner dynamics is one that turns around L_1.

In addition, different scattering maps, corresponding to different homoclinic manifolds, have different effects on action level sets. If several scattering maps are available, one may wish to choose at every step the scattering map that has the maximum effect on action level sets. We provide a practical procedure on how to select the scattering map at each step in order to obtain orbits that yield the largest change in the action variable with the fewest homoclinic excursions, i.e., the fewest number of turns around the Earth.

The main result, Theorem 2.4 assumes the existence of a 3-dimensional NHIM Λ_c near L_1, the existence of transverse homoclinic intersections of $W^s(\Lambda_c)$ and $W^u(\Lambda_c)$ — the stable and unstable manifolds of Λ_c —, and the existence of corresponding scattering maps on Λ_c. The dimension of the problem is further reduced by considering a suitable Poincaré section Σ and its corresponding first return map F. The reduced NHIM $\Lambda_c^\Sigma := \Lambda_c \cap \Sigma$, the induced scattering maps, and the induced inner dynamics — defined as the restriction $F_{\Lambda_c^\Sigma}$ of F to Λ_c^Σ —, are 2-dimensional. Theorem 2.4 says that if there exists a pseudo-orbit generated by applying one of the scattering maps alternatively with applying the inner dynamics for some number of iterates, then there exists a true orbit that follows that pseudo-orbit. Hence, once we find a pseudo-orbit that achieves a significant change in the action variable, there is a true orbit that also achieves a significant change in the action variable.

It does not seem possible to verify analytically all of the conditions required by Theorem 2.4 without imposing further restrictions on the parameter values of the model. However, the numerical verification of those conditions can be done easily and with high accuracy.

The level sets of the action variable in Λ_c^Σ are 1-dimensional action level sets (curves) in a 2-dimensional phase space. We construct recursively an ordered sequence of such curves, and verify that the image of each curve by a suitably chosen scattering map intersects the next curve in the sequence. Checking these intersections numerically is very easy, since the problem is low dimensional. Then we have to apply the inner dynamics to move from the image of one scattering map to a location where we can apply the next scattering map. From a numerical standpoint, these level sets are almost invariant, and $F_{\Lambda_c^\Sigma}$ restricted to each level set is nearly a rigid rotation, with the frequency varying from one level set to another. These properties allow movement along each level set without changing too much the value of the action. We successively apply a scattering map to each action level set, and follow it by a number of iterates of the inner dynamics to arrive to a suitable location where another application of a scattering map yields a jump to the next action level set. In this way, we obtain explicit constructions of pseudo-orbits. We note that these pseudo-orbits are indistinguishable from true orbits from a numerical standpoint.

Since our construction is explicit, we can track the diffusion time of each orbit obtained through this mechanism (here we are referring to the numerically computed orbits, which coincide with the pseudo-orbits that we construct). Additionally, we obtain information on how the diffusion range in the action variable varies with the energy level considered. We discover that energy levels close to that of L_1 yield a smaller diffusion range, and energy levels farther away from that of L_1 yield a wider diffusion range.

Our work can be viewed as a *semi-analytical approach*[1], by which we mean the following here. We have an analytical result, Theorem 2.4, which provides the existence of diffusing orbits under certain assumptions on the system. The assumptions fall into two categories. Some of them – the existence of a NHIM, the existence of homoclinic trajectories – can be verified analytically for certain values of the parameters of the problem – the mass ratio of the heavy bodies, the energy level –, but need to be verified numerically for realistic parameter values. Some other assumptions can only be verified numerically – the computation of the scattering map and of the inner map and its iterates. Also, the final construction of diffusing orbits is numerical.

A highlight of our approach is that the numerical verifications can in principle be validated through computer assisted proofs using interval arithmetic, via existing libraries developed for this type of problems, e.g., CAPD [23]. The implementation of computer assisted proofs is, however, beyond the scope of this paper.

5. Structure of the paper. In this paper we provide two types of results. In Section 2, after setting up the problem and introducing the methodology, we provide an abstract result, Theorem 2.4 , which gives some sufficient conditions, on a 5-dimensional, fixed energy manifold of the SCRTBP, for the existence of trajectories that visit some given sequence of action level sets in the prescribed order.

[1]A discussion about the meaning of the terms 'semi-analytical' and 'semi-numerical' appears in [5]; these terminologies are not standard.

The proof of Theorem 2.4, given in Section 3, relies on the theory of normal hyperbolicity, on the geometric properties of scattering maps, and on the Poincaré recurrence theorem. Relevant references to our approach include [6, 22, 21, 17, 33, 7].

The numerical verification of the conditions of the theorem is performed in Section 4 with high precision computations. We also obtain numerically orbits which visit a prescribed sequence of action level sets, and thus achieve diffusion.

6. Related works. The diffusion mechanism described above is similar to Arnold's mechanism of diffusion in nearly integrable Hamiltonian systems [1]. The Arnold diffusion problem claims that, small, 'generic' perturbations of integrable Hamiltonian systems of more than 2-degrees of freedom, yield trajectories that drift across a significant portion of the phase space. Genericity means that the perturbations are taken from an open and dense set of functions in a certain regularity class, or from a cusp residual class (see [45, 46]). It is often the case that one cannot verify whether a given perturbation belongs or not to such a generic class. Thus, such treatments are not particularly suitable to applications to concrete models – such as, those from celestial mechanics –, where the perturbation can be very specific.

The Arnold diffusion problem has a long history, and many important contributions include [13, 3, 27, 11, 12, 4, 59, 19, 39, 15, 30, 51]. Recent progress on the Arnold diffusion problem has been reported in [2, 40, 41, 10, 45, 46]. The approaches used in these works range from variational to geometric/topological. This paper is more in line with the geometric method developed in [21, 32, 31, 33].

The SCRTBP that we consider in this paper is a real-life model for the Arnold diffusion problem. Although its associated Hamiltonian system is not nearly-integrable *per se*, this model exhibits the same type of geometric structures and mechanisms as in the Arnold diffusion problem, as described above. We use this model to illustrate many of the difficulties of applying some of the well-known methods to concrete examples. More importantly, we use the SCRTBP to showcase the advantages of our method, which does not rely on the explicit knowledge of the inner dynamics and of the invariant objects that organize it. Indeed, our method relies mostly on understanding the outer dynamics, via scattering maps.

Arnold's mechanism of diffusion has been identified in other models from celestial mechanics. The existence of Arnold diffusion type of trajectories was shown via analytical methods in several models, e.g., [60, 61, 48, 56, 9]. Different mechanisms of diffusion in other celestial mechanics models have been established via combinations of analytical arguments and numerical experiments in [28, 29, 24, 62]. Related works discussing Arnold diffusion in the context of celestial mechanics include [42, 13, 14, 55].

2. Setup and main result

In this section we describe the spatial restricted three body problem (SCRTBP) and provide the main theoretical result on the existence of Arnold's mechanism of diffusion for this problem.

2.1. **The spatial circular restricted three-body problem.** The model is defined as follows: two main bodies rotate in the plane about their common center of mass in circular orbits under their mutual gravitational influence. A third body, of infinitesimal mass, moves in space attracted by the other two but not influencing

their motion. The problem is to describe the motion of this third body. A general reference for the SCRTBP is Szebehely's book [58].

Usually, the two rotating bodies are called the primaries. We will consider as primaries the Sun and the Earth. The third body can be regarded as a satellite or a spaceship of negligible mass. Notice that, unlike in the planar restricted problem, the motion of the third body is not restricted to the plane of motion of the two primaries.

We use a rotating system of coordinates centered at the center of mass. The plane X, Y rotates with the primaries. The primaries are on the X axis, the Y axis is perpendicular to the X axis and contained in the plane of rotation, and the angular velocity vector is normal to the plane along the Z axis.

In dimensionless coordinates, μ_1 and μ_2 represent the masses of the primaries. They satisfy the relation $\mu_1+\mu_2 = 1$. Let the smaller mass be $\mu_2 = \mu$ and the larger one be $\mu_1 = 1-\mu$. The distance between the primaries is also 1. In the sequel, we will focus on the Sun-Earth system for which $\mu = 3.040423398444176 \times 10^{-6}$. The Sun is located to the right of the origin at $P_1 = (\mu, 0, 0)$, and the Earth is located to the left at $P_2 = (\mu - 1, 0, 0)$. See Figure 1.

The equations of motion of the third body, using dimensionless variables, are

$$\ddot{X} - 2\dot{Y} = \Omega_X, \tag{2.1a}$$

$$\ddot{Y} + 2\dot{X} = \Omega_Y, \tag{2.1b}$$

$$\ddot{Z} = \Omega_Z, \tag{2.1c}$$

where

$$\Omega = \frac{1}{2}(X^2 + Y^2) + \frac{1-\mu}{r_1} + \frac{\mu}{r_2} + \frac{1}{2}\mu(1-\mu),$$

and r_1, r_2 denote the distances from the third body to the larger and to the smaller primary, respectively:

$$r_1^2 = (X-\mu)^2 + Y^2 + Z^2,$$
$$r_2^2 = (X-\mu+1)^2 + Y^2 + Z^2.$$

These equations have an integral of motion [58] called the Jacobi integral

$$C = 2\Omega - (\dot{X}^2 + \dot{Y}^2 + \dot{Z}^2).$$

The equations of motion take Hamiltonian form if we consider positions X, Y, Z and momenta $P_X = \dot{X} - Y$, $P_Y = \dot{Y} + X$, $P_Z = \dot{Z}$. The Hamiltonian is

$$H = \frac{1}{2}(P_X^2 + P_Y^2 + P_Z^2) + YP_X - XP_Y - \frac{1-\mu}{r_1} - \frac{\mu}{r_2} - \frac{1}{2}\mu(1-\mu). \tag{2.2}$$

The Hamiltonian and the Jacobi integral are simply related by $H = -\frac{C}{2}$. In this paper, we will use the Jacobi integral instead of the Hamilton integral.

Due to the Jacobi integral, the dimensionality of the space can be reduced by one. Trajectories of equations (2.1) stay on the energy surface M given by

$$M = \{C(X, Y, Z, \dot{X}, \dot{Y}, \dot{Z}) = c\}. \tag{2.3}$$

which is a 5-dimensional submanifold of $\mathbb{R}^6$.

The system of equations (2.1) has five equilibrium points. Three of them, denoted L_1, L_2 and L_3, lie on the X axis and are usually called the 'collinear' equilibrium points (see Figure 1). Notice that we denote by L_1 the interior collinear point, located between the primaries.

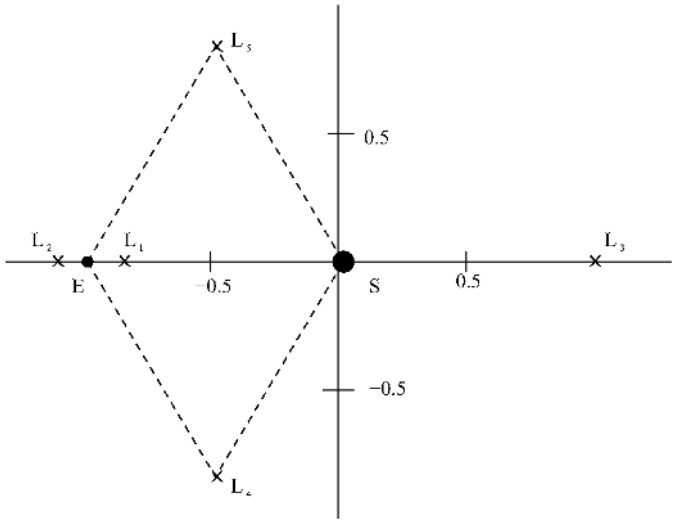

FIGURE 1. The position of the libration points relative to Sun and Earth.

2.2. **Dynamics near L_1.** The linearized dynamics around each of the three collinear equilibrium points is of type saddle × center × center for all values of μ. In particular, the linearized system at L_1 has eigenvalues of the type $\pm\lambda, \pm i\nu, \pm i\omega$. For each Jacobi constant c which is below $c_1 := C(L_1)$ (the Jacobi constant at L_1) but sufficiently close to it, the linearized system restricted to the corresponding energy level contains a 3-dimensional sphere that is normally hyperbolic, and is filled with periodic orbits and quasi-periodic orbits lying on 2-dimensional invariant tori. The definition of a normally hyperbolic invariant manifold is given in Section 2.5. By the Center Manifold Theorem (see e.g., [57]), there exists a 4-dimensional invariant center manifold $W^c(L_1)$ that is tangent at L_1 to the generalized eigenspace E^c corresponding to $\pm i\nu, \pm i\omega$, and is locally a graph over E^c near L_1. In general, the center manifold is not necessarily unique, but every center manifold contains any solution that stays for all time inside a sufficiently small neighborhood of L_1. Hence, every center manifold contains any compact invariant set within some sufficiently small neighborhood of L_1. Also, $W^c(L_1)$ is C^r-differentiable for any $r < \infty$.

Since $W^c(L_1)$ is a graph over E^c, the restriction of C to $W^c(L_1)$ can be locally expressed in terms of the coordinates induced from E^c. Since $C_{|W^c(L_1)}$ has a local maximum point at L_1, and the Hessian D^2C at L_1 is negative definite, L_1 is a non-degenerate local maximum point. By the Morse Lemma, on $W^c(L_1)$ there exists a local coordinate system (u_1, u_2, u_3, u_4) centered at L_1, such that

$$C_{|W^c(L_1)}(u_1, u_2, u_3, u_4) = c_1 - u_1^2 - u_2^2 - u_3^2 - u_4^2.$$

Thus, the intersection between $W^c(L_1)$ and every energy manifold $\{C = c\}$, with $c \in [c_1 - \epsilon, c_1)$, with $\epsilon > 0$ sufficiently small, is a 3-dimensional sphere that is a normally hyperbolic invariant manifold for the Hamiltonian flow restricted to that energy manifold. Since this 3-sphere is compact and invariant, it is also uniquely determined. This argument appears, e.g., in [49].

The above discussion about the uniqueness property of the center manifold implies that the portion of $W^c(L_1)$ corresponding to Jacobi constants in $[c_1 - \epsilon, c_1]$, with $\epsilon > 0$ sufficiently small, is also uniquely determined.

Recall that the normally hyperbolic 3-sphere for the linearized system near L_1 is filled with 2-dimensional invariant tori. The KAM theorem can be applied to show the existence of a KAM family of 2-dimensional invariant tori survives from the linear case to the non-linear case; see [56]. We emphasize that the Center Manifold Theorem and the KAM theorem only apply for Jacobi constants very close to the critical value c_1. In the sequel, we will consider Jacobi constants that are below but not very close to the Jacobi constant $c_1 = 3.00090$ of L_1, and above the Jacobi constant $c_{halo} = 3.00082$ where *halo* orbits appear. These halo orbits are periodic, three-dimensional orbits that bifurcate from the planar Lyapunov periodic orbits when the energy reaches certain level $c_{halo} < c_1$, and appear as a pair of symmetric fixed points in the Poincaré section $z = 0$. See [35].

In the sequel, we will explore two fixed values of the Jacobi constant, $c = 3.00082$ and $c = 3.00088$. Neither constant is sufficiently close to L_1 so that we can apply the analytical results mentioned above. Instead, we will use a Birkhoff normal form to approximate numerically the center manifold $W^c(L_1)$ and the normally hyperbolic invariant manifold $\Lambda_c = W^c(L_1) \cap \{C = c\}$. See Subsection 4.1.1. A rigorous proof for the existence of the normally hyperbolic invariant manifold for a fixed value of the Jacobi constant could in principle be obtained by using computer assisted techniques in the style of [8]. The Birkhoff normal form provides an approximation of the Hamiltonian H by an integrable hamiltonian H_N, $N \geq 2$. Therefore, in the normal form, on a fixed energy level, there exists a normally hyperbolic invariant manifold S_c, which is diffeomorphic to a three-sphere and is filled with invariant tori. Also, the Birkhoff normal form provides an action-angle coordinate system $(I_p, I_v, \phi_p, \phi_v)$ on some neighborhood of L_1 in $W^c(L_1)$. We can choose this coordinate system so that I_v represents the out-of-plane amplitude of a quasi-periodic motion. The energy condition $C = c$ yields I_p as an implicit function of I_v, ϕ_p, ϕ_v, c. For each fixed value the out-of-plane action $I_v = \bar{I} = \text{const.}$, there is a unique invariant torus for the normal form

$$T_{\bar{I}} = \{(I_v, \phi_p, \phi_v) \in S_c \,|\, I_v = \bar{I}\}.$$

Of course, when the Jacobi constant is not assumed to be sufficiently close to c_1, we cannot obtain analytically the persistence of a normally hyperbolic invariant manifold diffeomorphic to a three-sphere for the original Hamiltonian, or the invariant tori contained inside the three-sphere.

In the sequel, we will make the following assumptions:

(1) There exists $\epsilon_0 > 0$ sufficiently small such that for each value of $c \in [c_{halo} + \epsilon_0, c_1)$ there exists a normally hyperbolic invariant manifold Λ_c diffeomorphic to the three-sphere S_c, which is contained in the energy manifold $\{C = c\}$;
(2) The diffeomorphism $\mathsf{h} : S_c \to \Lambda_c$ from (1) is ϵ_1-close to the identity, for some $\epsilon_1 > 0$ sufficiently small, that is $\|\mathsf{h} - \mathrm{id}_{S_c}\|_{C^0} < \epsilon_1$;
(3) The center manifold $W^c_{loc}(L_1) := \bigcup_{c \in [c_{halo} + \epsilon_0, c_1]} \Lambda_c$ is symplectic, that is, the restriction of the standard symplectic form on $W^c(L_1)$ is non-degenerate.

Via the diffeomorphism h from (2), the coordinate system (I_v, ϕ_p, ϕ_v) on S_c can be carried out to a coordinate system on Λ_c, which, to avoid an overburdening of the notation, we still denote (I_v, ϕ_p, ϕ_v). We note that, while a level set $I_v = \text{const.}$ is an invariant torus in S_c, it is not an invariant set in Λ_c; nevertheless, the level set $I_v = \text{const.}$ in Λ_c is ϵ_1-close to the corresponding invariant torus.

2.3. **Homoclinic connections.** The stable and unstable manifolds $W^s(\Lambda_c)$, $W^u(\Lambda_c)$ of Λ_c, are 4-dimensional manifolds contained in the 5-dimensional energy manifold $C = c$, and they are foliated by 1-dimensional fibers $W^s(x)$, $W^u(x)$, $x \in \Lambda_c$, respectively; these fibers are equivariant under the Hamiltonian flow. Also, for each level set $\mathcal{L}_{\bar{I}} = \{(I_v, \phi_p, \phi_v) \in \Lambda_c \,|\, I_v = \bar{I}\}$, we can define the sets

$$W^u(\mathcal{L}_{\bar{I}}) = \bigcup_{x \in \mathcal{L}_{\bar{I}*}} W^u(x),\ W^s(\mathcal{L}_{\bar{I}}) = \bigcup_{x \in \mathcal{L}_{\bar{I}}} W^s(x).$$

Due to the smooth dependence of these fibers on base points, these sets are C^ℓ-differentiable manifolds for some $\ell \geq 1$, but not invariant. We will select some energy levels c within the range $c \in [c_{halo} + \epsilon_0, c_1)$ and we will show numerically that $W^u(\Lambda_c)$ intersects transversally $W^s(\Lambda_c)$ in the energy manifold. Moreover, we will show that there exists a range $[I_a, I_b]$ of I_v-action level sets, which depends on c, such that, for each $\bar{I} \in [I_a, I_b]$, there exists $I' \in [I_a, I_b]$, such that $W^u(\mathcal{L}_{\bar{I}})$ has transverse intersections with $W^s(\mathcal{L}_{I'})$. The level set I' can be chosen above or below the initial level $\bar{I}$. Such a transverse intersections imply that there exists a pair of points $x_- \in \mathcal{L}_{\bar{I}}$, $x_+ \in \mathcal{L}_{I'}$, such that $W^u(x_-)$ intersects $W^s(x_+)$ at some point $x \in W^u(\mathcal{L}_{\bar{I}}) \cap W^s(\mathcal{L}_{I'})$. One can define an associated scattering map given by $x_- \mapsto \sigma(x_-) := x_+$; the scattering map σ is a local diffeomorphism defined on some open set of Λ_c. See Section 2.5.

We note that if $W^u(\mathcal{L}_{\bar{I}})$ has transverse intersection with $W^s(\mathcal{L}_{I'})$, it also has transverse intersection with all $W^s(\mathcal{L}_{I'})$ with I' sufficiently close to I'. We stress again that the I_v-level sets $\mathcal{L}_{\bar{I}}$ are not necessarily invariant, but they are 'almost invariant'.

Using these facts we can construct transition chains of level sets. Given a collection of scattering maps σ_i, $i = 1, \ldots, K$, by a transition chain of level sets we mean a sequence of level sets $\{\mathcal{L}_{I_j}\}_{j=1,\ldots,N}$ in Λ_c, with $I_j \in [I_a, I_b]$, satisfying the following properties:

(1) for each j, there exists a point $x_j \in \mathcal{L}_{I_j}$ and a scattering map $\sigma_{i(j)}$, with x_j in the domain of $\sigma_{i(j)}$, such that that $\sigma_{i(j)}(x_j) = x'_{j+1} \in \mathcal{L}_{I'_{j+1}}$, with $I'_{j+1} \approx I_{j+1}$;
(2) there exists $t_{j+1} > 0$ such that $\Phi^{t_{j+1}}_{|\Lambda_c}(x'_{j+1}) = x_{j+1}$ with $x_{j+1} \in \mathcal{L}_{I_{j+1}}$, where $\Phi^t_{|\Lambda_c}$ denotes the Hamiltonian flow restricted to Λ_c;
(3) the point x_{j+1} is in the domain of some scattering map $\sigma_{i(j+1)}$, and $\sigma_{i(j+1)}(x_{j+1}) \in \mathcal{L}_{I_{j+2}}$.

This construction is made precise in Section 2.6.

2.4. **Normally hyperbolic invariant manifolds.** We recall the definition and some basic properties of normally hyperbolic invariant manifolds, following [52, 25].

Consider a C^r-differentiable flow $\Phi : M \times \mathbb{R} \to M$, $r \geq 2$, defined on an m-dimensional manifold M.

Assume that there exists a normally hyperbolic invariant manifold $\Lambda \subseteq M$ which is n_c-dimensional, and the stable and unstable bundles have dimensions n_s, n_u, respectively, and $m = n_c + n_u + n_s$. By Λ being a normally hyperbolic invariant manifold for Φ^t we mean that Λ is compact n_c-dimensional submanifold of M that is invariant under Φ^t, and there exists a splitting of the tangent bundle of TM into sub-bundles

$$TM = E^{n_u} \oplus E^{n_s} \oplus T\Lambda,$$

that are invariant under $D\Phi^t$ for all $t \in \mathbb{R}$, and there exist a constant $C > 0$ and rates $0 < \beta < \alpha$, such that for all $x \in \Lambda$ we have

$$\begin{aligned}
\|D\Phi^t(x)(v)\| &\leq Ce^{-\alpha t}\|v\| \text{ for all } t \geq 0, \text{ if and only if } v \in E^{n_s}_x,\\
\|D\Phi^t(x)(v)\| &\leq Ce^{\alpha t}\|v\| \text{ for all } t \leq 0, \text{ if and only if } v \in E^{n_u}_x,\\
\|D\Phi^t(x)(v)\| &\leq Ce^{\beta|t|}\|v\| \text{ for all } t \in \mathbb{R}, \text{ if and only if } v \in T_x\Lambda.
\end{aligned}$$

The manifold Λ is C^ℓ-differentiable for some $\ell \leq r - 1$ that depends in some explicit way on r, α, and β. We will assume that $\ell \geq 2$. There exist stable and unstable manifolds of Λ, denoted $W^s(\Lambda)$ and $W^u(\Lambda)$, respectively, that are $C^{\ell-1}$-differentiable, which are foliated by stable and unstable manifolds of points, respectively. For each $x \in W^u(\Lambda)$ there exists a unique $x_- \in \Lambda$ such that $x \in W^u(x_-)$, and for each $x \in W^s(\Lambda)$ there exists a unique $x_+ \in \Lambda$ such that $x \in W^s(x_+)$. We define the wave maps $\Omega_+ : W^s(\Lambda) \to \Lambda$ by $\Omega_+(x) = x_+$, and $\Omega_- : W^u(\Lambda) \to \Lambda$ by $\Omega_-(x) = x_-$. The maps Ω_+ and Ω_- are C^ℓ-differentiable.

2.5. **Scattering map.** Consider the setting from the previous section. Assume that $W^u(\Lambda)$ has a transverse intersection with $W^s(\Lambda)$ along a n_c-dimensional homoclinic manifold Γ.

In the sequel we recall the scattering map, and some of its properties from [21].

We start with providing an intuitive explanation. Let x be a homoclinic point in Γ. The normal hyperbolicity of Λ implies that there is a unique point $x_- \in \Lambda$ such that the backwards orbit of x approaches the backwards orbit of x_- in Λ, and that there is a unique point $x_+ \in \Lambda$ such that the forward orbit of x approaches the forward orbit of x_+ in Λ. Equivalently, x belongs to a uniquely defined unstable fiber $W^u(x_-)$. The scattering map is, by definition, the map defined by $x_- \in \Lambda \mapsto x_+ \in \Lambda$, as the point $x \in \Gamma$ is varied. In order for this to be a well defined map, the homoclinic manifold has to satisfy certain conditions, which are detailed below. The resulting map is, in general, not defined on the whole of Λ, but only on some open subset of it.

The main role of the scattering map is to encode in a simple way, the backwards and the forward asymptotic behavior of homoclinic orbits. For example, suppose that the backwards orbit of a homoclinic point x accumulates onto some invariant torus $\mathcal{T}_-$, and that forward orbit of x accumulates onto some other invariant torus $\mathcal{T}_+$. The corresponding scattering map will assign to a certain point $x_- \in \mathcal{T}_-$ a certain other point $x_+ \in \mathcal{T}_+$.

Now we proceed to the formal definition of the scattering map.

First, we list conditions regarding the transverse intersection of $W^u(\Lambda)$ with $W^s(\Lambda)$ along Γ. The fact that the intersection of these manifolds is transverse

means that for each $x \in \Gamma \subseteq W^u(\Lambda) \cap W^s(\Lambda)$, we have

$$\begin{aligned} T_x M &= T_x W^u(\Lambda) + T_x W^s(\Lambda), \\ T_x \Gamma &= T_x W^u(\Lambda) \cap T_x W^s(\Lambda). \end{aligned} \tag{2.4}$$

We further assume a strong transversality condition, that for each $x \in \Gamma$ we have

$$\begin{aligned} T_x W^s(\Lambda) &= T_x W^s(x_+) \oplus T_x(\Gamma), \\ T_x W^u(\Lambda) &= T_x W^u(x_-) \oplus T_x(\Gamma), \end{aligned} \tag{2.5}$$

where x_-, x_+ are the uniquely defined points in Λ corresponding to x.

The restrictions Ω_+^Γ, Ω_-^Γ of Ω_+, Ω_-, respectively, to Γ are local $C^{\ell-1}$ - diffeomorphisms.

Second, we restrict Γ, if necessary, so that Ω_+^Γ, Ω_-^Γ are $C^{\ell-1}$-diffeomorphisms. A homoclinic manifold Γ for which the corresponding restrictions of the wave maps are $C^{\ell-1}$-diffeomorphisms will be referred as a *homoclinic channel*.

Definition 2.1. Given a homoclinic channel Γ, the scattering map associated to Γ is the $C^{\ell-1}$-diffeomorphism $\sigma^\Gamma = \Omega_+^\Gamma \circ (\Omega_-^\Gamma)^{-1}$ from the open subset $\Omega_-^\Gamma(\Gamma)$ in Λ to the open subset $\Omega_+^\Gamma(\Gamma)$ in Λ.

This formal definition agrees with the explanation given at the beginning of the section. If $x \in \Gamma$ is a homoclinic point, then $(\Omega_-^\Gamma)^{-1}(x) = x_-$ represents the foot point of the stable fiber $W^u(x_-)$ containing x, and $\Omega_+^\Gamma(x) = x_+$ represents the foot point of the stable fiber $W^s(x_+)$ containing x. Thus $\sigma^\Gamma(x_-) = \Omega_+^\Gamma \circ (\Omega_-^\Gamma)^{-1}(x_-) = \Omega_+^\Gamma(x) = x_+$.

We recall below one important property of the scattering map which will be used in the future.

Proposition 2.2. *Assume that M is endowed with a symplectic (respectively exact symplectic) form ω and that $\omega_{|\Lambda}$ is also symplectic (we implicitly assume that $n_u = n_s$, and $n_c \geq 2$ is an even number). Assume that Φ^t is symplectic (respectively exact symplectic). Then, the scattering map σ^Γ is symplectic (respectively exact symplectic).*

2.6. **Main analytical results.**

Proposition 2.3. *Consider the spatial circular restricted three-body problem with the mass ratio μ as in the Sun-Earth system model. Let c be a fixed Jacobi constant. Assume that there exists a normally hyperbolic invariant manifold $\Lambda = \Lambda_c$ about L_1, for the flow generated by (2.1), which is diffeomorphic to a 3-dimensional sphere.*

Assume that $W^u(\Lambda_c)$ intersects transversally $W^s(\Lambda_c)$ in the energy manifold along a finite family of homoclinic channels Γ_i, where $i = 1, \ldots, k$. Let σ_i be the scattering map associated to Γ_i, $i = 1, \ldots, k$,

$$\sigma_i : \Omega_-^{\Gamma_i}(\Gamma_i) \to \Omega_+^{\Gamma_i}(\Gamma_i).$$

Let (I_v, ϕ_p, ϕ_v) be an action-angle coordinate system on Λ_c derived from the Birkhoff normal form (see Section 4.1.1), with I_v representing the out-of-plane amplitude.

Let Σ be a Poincaré surface of section given by $\{\phi_p = 0, \dot{\phi}_p > 0\}$, and let F be the first return map to Σ.

Let $\Lambda_c^\Sigma = \Lambda_c \cap \Sigma$. Assume that Λ_c^Σ can be parametrized as follows:

$$\Lambda_c^\Sigma = \{(I, \phi) \,|\, I \in [0, I_{max}],\, \phi \in [0, 2\pi]\},$$

where $(I, \phi) = (I_v, \phi_v)$, and I_{max} represents the maximal value of the out-of-plane amplitude I_v of an orbit in Λ_c.

Then Λ_c^Σ is a NHIM for F, and $\Gamma_i^\Sigma = \Gamma_i \cap \Sigma$, $i = 1, \ldots, k$, is a homoclinic channel that determines a scattering map σ_i^Σ defined on some open subset of Λ^Σ. The relation between σ_i^Σ and σ_i is

$$\sigma_i^\Sigma = P_+^{\Gamma_i} \circ \sigma_i \circ \left(P_-^{\Gamma_i}\right)^{-1},$$

where $P_\pm^{\Gamma_i} : \Omega_\pm(\Gamma_i) \to \Omega_\pm(\Gamma_i^\Sigma)$ is given by $P_\pm^{\Gamma_i}(x_\pm) = \Phi^{\tau(x_\pm)}(x_\pm)$, where $\tau(x_\pm)$ is the first instant of time when the flow trajectory $\Phi^t(x_\pm)$ intersects Σ.

We will denote by $\mathcal{L}_{\bar{I}}$ the level set $\{I = \bar{I}\}$ in Λ_c, and by $\mathcal{L}_{\bar{I}}^\Sigma$ the level set $\{I = \bar{I}\}$ in Λ_c^Σ. Also we will denote by $B_{\bar{\delta}}(\bar{I}, \bar{\phi})$ a topological disk in Λ_c^Σ that contains the point $(\bar{I}, \bar{\phi})$ and has diameter less than $\bar{\delta} > 0$.

Theorem 2.4. *Assume we are in the situation described in Proposition 2.3. Let $\delta > 0$.*

Assume that there exists a finite sequence I_j of level sets of I, with $0 < I_j < I_{max}$, a finite sequence δ_j of positive reals, with $0 < \delta_j < \delta/2$, such that the following property is satisfied for each $j = 0, \ldots, N-1$:

(i) *there exists a scattering map $\sigma_{i(j)}^\Sigma$ and a point $(I_j, \phi_j) \in \mathcal{L}_{I_j}^\Sigma$ such that $B_{\delta_j}(I_j, \phi_j)$ is contained in the domain of $\sigma_{i(j)}^\Sigma$,*

(ii) *there exists $k_j > 0$ such that*

$$int[F^{k_j} \circ \sigma_{i(j)}^\Sigma(B_{\delta_j}(I_j, \phi_j))] \supseteq B_{\delta_{j+1}}(I_{j+1}, \phi_{j+1}). \tag{2.6}$$

Then there exist an orbit z_j of F in Σ, $j = 0, \ldots, N$, and a sequence of positive integers $n_j > 0$, $j = 0, \ldots, N-1$, such that $z_{j+1} = F^{n_j}(z_j)$ and

$$d(z_j, \mathcal{L}_{I_j}^\Sigma) < \delta/2, \text{ for all } j = 0, \ldots, N. \tag{2.7}$$

Consequently, there exist a trajectory $\Phi^t(z)$ of the Hamiltonian flow, and a finite sequence of times $0 = t_0 < t_1 < t_2 < \ldots < t_N$, such that

$$d(\Phi^{t_j}(z), \mathcal{L}_{I_j}) < \delta. \tag{2.8}$$

Remark 2.5. We will see in the proof of Theorem 2.4, which is given below, that the condition (2.6) allows us to construct pseudo-orbits for the iterated function system determined by the map F and by the scattering maps σ_i^Σ's, for $i = 1, \ldots, k$. These pseudo-orbits visit the successive balls $B_{\delta_j}(I_j, \phi_j)$, $j = 0, \ldots, N$. Then, we will use the topological shadowing type of result, Lemma 3.1, to prove that such pseudo-orbits are shadowed by true orbits.

Remark 2.6. In our model, we will only be able produce a finite sequence I_j of I-level sets that starts at some initial value $I_a > 0$ and ends at some final value I_b, with $I_b < I_{max}$. We will be able to choose I_a as close to 0 as we wish, however how close we are able to choose I_b to I_{max} depends quite dramatically on the Jacobi constant c. For c close to c_1 (the Jacobi constant of L_1) we can only choose values of I_b that are significantly smaller than I_{max}. When the c-value is increased, the values of I_b that we can choose get closer to I_{max}. This implies that for a suitably high energy levels we are able to construct trajectories whose out-of-plane amplitude increases from nearly 0 to a significantly large fraction of I_{max}.

Here we should also mention that we have a investigated in detail only scattering maps corresponding to first-cut homoclinics, obtained at the first-intersections of

the stable and unstable manifolds with the surface of section of choice Σ. Nevertheless, 2-nd or 3-rd cut homoclinics did not seem to make much of a difference. More details are provided in Section 4.

It is not possible to choose the initial value $I_a = 0$, since this corresponds to the planar problem $z = 0$. The level set $I_v = 0$ represents a periodic orbit about L_1, known as the horizontal Lyapunov orbit. Since $z = 0$ is an invariant set for the flow, all trajectories with zero initial out-of-plane amplitude remain at this level for all time.

Also, generically it is not possible to obtain a final value $I_b = I_{max}$. The level set $I_v = I_{max}$ corresponds geometrically to the so called vertical Lyapunov orbit, which is 1-dimensional, hence its stable and unstable manifolds are 2-dimensional; 2-dimensional manifolds do not generically intersects in a 5-dimensional energy manifold.

Remark 2.7. We note that Theorem 2.4 requires very coarse information about the inner dynamics, restricted to the NHIM. We do not need to know about the existence of KAM tori and about the size of the gaps between such tori. We do not need to verify whether $F_{\Lambda_c^\Sigma}$ on Λ_c^Σ verifies a twist condition, or the existence of many topologically transitive invariant tori and/or of Aubry-Mather sets. Although such geometric objects are quite apparent in the numerical investigations, providing analytical arguments or computer assisted proofs to show their existence is laborious. Our key point is that it is not necessary to detect transition chains formed by the stable and unstable manifolds of KAM tori, since diffusing orbits only follow them for finite time anyway. Transition chains formed by almost invariant sets – such as the level sets of the action variable – and their associated stable and unstable manifolds, are sufficient to establish the existence of diffusing orbits. Moreover, the assumptions required by Theorem 2.4 are rather mild and easy to verify numerically. Condition (i) amounts to the calculation of scattering maps and of their domains. For condition (ii) we first verify that the image of a level set $\mathcal{L}^\Sigma_{I_j}$ – which is a curve – via one of the scattering map intersects the next level set $\mathcal{L}^\Sigma_{I_{j+1}}$ – which is another curve – within the 2-dimensional phase space. Hence we can choose a ball around a point in $\mathcal{L}^\Sigma_{I_j}$ that is mapped by the scattering map onto a ball around $\mathcal{L}^\Sigma_{I_{j+1}}$. Since from a numerical standpoint the level set $\mathcal{L}^\Sigma_{I_{j+1}}$ is almost invariant, and $F_{\Lambda_c^\Sigma}$ restricted to it is nearly a rigid rotation, we then verify that there the image under some number of iterations of $F_{\Lambda_c^\Sigma}$ of the latter ball around $\mathcal{L}^\Sigma_{I_{j+1}}$ contains inside it another ball around $\mathcal{L}^\Sigma_{I_{j+1}}$, which subsequent image by some scattering map intersects $\mathcal{L}^\Sigma_{I_{j+2}}$. The sizes of these balls can be adjusted so that the inclusion of a ball inside another ball can be done well within the margin of error. Thus, the numerical verification of the conditions (i) and (ii) of Theorem 2.4 is simple and can be done with large precision. More details are provided in Section 4.

Remark 2.8. In the statement of Theorem 2.4 the order of the iterates n_j that appear in the conclusion of the theorem is different from the order of the iterates k_j that appear in (2.6). As we will see in Section 3, our proof for the existence of a true orbit of the type $z_{j+1} = F^{n_j}(z_j)$ requires invoking Poincaré recurrence theorem. Thus, the above theorem does not yield quantitative information on the time required for these orbits to drift. However, in the numerical experiments, we can estimate numerically the recurrence time, and we can choose k_j large enough

so that it takes into account this recurrence time; hence, at the end, we can obtain $n_j = k_j$. Also note that the above theorem allows to use several scattering maps. Thus, at each step of the construction of the chain of level sets $\mathcal{L}^{\Sigma}_{I_j}$, given I_j one can always choose a scattering map $\sigma^{\Sigma}_{i(j)}$ that, when applied to the level set $\mathcal{L}^{\Sigma}_{I_j}$ reaches another level set $\mathcal{L}^{\Sigma}_{I_{j+1}}$ with I_{j+1} the furthest possible from I_j, and in the desired direction (i.e, either above or below I_j). More details are provided in Section 4.

3. Proofs of the main results

3.1. **Preliminaries.** Consider the general case of a discrete dynamical system given by a C^r-smooth map F on a compact, C^r-smooth manifold M. Assume that Λ is a normally hyperbolic invariant manifold (NHIM) in M. Suppose that there exists a finite collection of homoclinic channels $\Gamma_i \subseteq M$, for $i \in \{1, \dots, k\}$, for some positive integer k. Let $\sigma_i : \Omega_-(\Gamma_i) \to \Omega_+(\Gamma_i)$ be the scattering map associated to Γ_i, for $i \in \{1, \dots, k\}$.

Lemma 3.1 ([33])**.** *Assume that $F : M \to M$ is a C^r-map, $r \geq 3$, $\Lambda \subseteq M$ and $\Gamma_i \subseteq M$ are as above, and σ_i is the scattering map corresponding to the homoclinic channel Γ_i, for $i \in \{1, \dots, k\}$.*

Then, for every $\varepsilon > 0$ and every pseudo-orbit $\{y_i\}_{i\geq 0}$ in Λ of the form

$$y_{i+1} = F^{m_i} \circ \sigma_{i(j)} \circ F^{n_i}(y_i), \quad i \geq 0$$

with $n_i \geq n^*$, for some n^* depending on ε, and $m_i \geq m_i^*$, for some m_i^* depending on ε and on the powers $n_0, \dots, n_{i-1}, n_i, m_0, \dots, m_{i-1}$, there exists an orbit $\{z_i\}_{i\geq 0}$ of F in M such that, for all $i \geq 0$,

$$z_{i+1} = F^{m_i+n_i}(z_i), \text{ and } d(z_i, y_i) < \varepsilon.$$

The proof of this lemma appears in [33].

3.2. **Proof of Proposition 2.3.** The proof is the same as for Proposition 3 in [17].

3.3. **Proof of Theorem 2.4.** The proof is very similar to that of Theorem 3.2 in [33].

Since the system that we consider is Hamiltonian, the center manifold $W^c(L_1)$ is symplectic. This implies that Λ^{Σ}_c is symplectic, and $F_{\Lambda^{\Sigma}_c}$ is a symplectic map. See [47, 43]. Moreover, each scattering map $\sigma_{i(j)}$ is symplectic [21]. Thus $F_{\Lambda^{\Sigma}_c}$ and $\sigma_{i(j)}$ preserve the area form induced by the symplectic structure on Λ^{Σ}_c, which gives rise to a measure μ on Λ^{Σ}_c that is absolutely continuous with respect to Lebesgue measure. In particular, $F_{\Lambda^{\Sigma}_c}$ and $\sigma_{i(j)}$ satisfy the so called Luzin N property, that the image of a zero measure set is a zero measure set.

Denote:

$$B_0 = B_{\delta_0}(I_0, \phi_0),$$

$$B_{j+1} = B_{\delta_{j+1}}(I_{j+1}, \phi_{j+1}) \subseteq F^{k_j} \circ \sigma_{i(j)}(B_j) = F^{k_j} \circ \sigma_{i(j)}(B_{\delta_j}(I_j, \phi_j)),$$

for $j = 0, \dots, N-1$.

We start with some preliminary remarks.

By the Poincaré Recurrence Theorem, μ-a.e. point in Λ^{Σ}_c is recurrent for $F := F_{\Lambda^{\Sigma}_c}$.

Assume that B is a ball in Λ^{Σ}_c, and that R is a full measure subset of B. Fix some k^* sufficiently large.

Applying the Poincaré Recurrence Theorem to F^{k^*} implies that the set

$$R^{k^*} = \{y \in R \,|\, F^{k^* \cdot t}(y) \in B \text{ for some } t \geq 1\}$$

has full measure in B. For $y \in R^{k^*}$ let $t_{min} = t_{min}(y)$ denote the time of the first return of y to B, that is

$$t_{min} = \min\{t \geq 1 \,|\, y \in R^{k^*} \text{ and } F^{k^* \cdot t}(y) \in B\}.$$

Denote $\hat{R}^{k^*} = \{F^{k^* \cdot t_{min}}(y) \,|\, y \in R\}$ the collection of the first returns of points of R to B under the iterates of F^{k^*}. We claim that $\hat{R}^{k^*}$ also has full measure in B, as we show below.

Let $\Theta = \{\tau \geq 1 \,|\, \exists y \in R^{k^*} \text{ s.t. } t_{min}(y) = \tau\}$ be the set of first return times to B, and, for each $\tau \in \Theta$, let $C_\tau = \{y \in R^{k^*} \,|\, t_{min}(y) = \tau\}$ be the set of points with a prescribed first return time $\tau \in \Theta$. Then $R^{k^*} = \bigcup_{\tau \in \Theta} C_\tau$, with the sets C_τ mutually disjoint. The sets $F^{k^* \cdot \tau}(C_\tau)$ are also mutually disjoint subsets in B; otherwise we would have $F^{k^* \cdot \tau}(y) = F^{k^* \cdot \tau'}(y')$ for some $1 \leq \tau < \tau'$ and $y \in C_\tau$, $y' \in C_{\tau'}$, so $F^{k^* \cdot (\tau' - \tau)}(y') = y \in B$ where $1 \leq \tau' - \tau < \tau'$, which is in contradiction with the definition of $\tau' = t_{min}(y')$. Since the sets $F^{k^* \cdot \tau}(C_\tau)$'s are mutually disjoint and F is measure preserving, $\mu(C_\tau) = \mu(F^{k^* \cdot \tau}(C_\tau))$ for $\tau \in \Theta$, hence the set $\hat{R}^{k^*} = \bigcup_{\tau \in \Theta} F^{k^* \cdot \tau}(C_\tau)$ is of full measure set in B, as claimed.

Thus, every point in $R^{k^*} \subseteq B$ returns to a point in $\hat{R}^{k^*} \subseteq B$ after some positive number of iterates of F^{k^*}. In terms of F, every point in $R^{k^*} \subseteq B$ gets mapped onto a point in $\hat{R}^{k^*} \subseteq B$ after at least k^* iterates. We will keep in mind that both R^{k^*} and $\hat{R}^{k^*}$ have full measure in B.

Now consider a scattering map σ, and let $F^{k'^*}$ be some iterate of F. Also let B' be a ball contained in $(F^{k'^*} \circ \sigma)(B)$, the image of B via $F^{k'^*} \circ \sigma$. Since σ and $F^{k'^*}$ are measure preserving, hence satisfy Luzin N property, the set $\hat{R}_j^{k^*}$ having a full measure in B implies that the set $(F^{k'^*} \circ \sigma)(\hat{R}^{k^*}) \cap B'$ has full measure in B'.

Now, starting from B_0, we will construct a tower of positive measure subsets of B_0 that are mapped onto full measure subsets of B_j, $j = 0, \ldots, N$, under successive applications of sufficiently large powers F^{k^*} and of $\sigma_{i(j)}$. The successive powers F^{k^*} will be adjusted at each step, and will be chosen large enough so they satisfy the conditions imposed by the shadowing result – Lemma 3.1.

More precisely, we make the following inductive construction. Let $\varepsilon = \delta/2$, with δ as in Theorem 2.4. Start with the set B_0.

For the initial step, set $R_0 = B_0$. Let n^* and m_0^* depending on ε as in Lemma 3.1, and let

$$\Sigma_0 = R_0^{n_0} \subseteq B_0, \text{ and } \hat{R}_0^{n_0} \subseteq B_0.$$

Note that $R_0' := [F^{k_0} \circ \sigma_{i(0)}(\hat{R}^{n_0})] \cap B_1$ has full measure in B_1. Consider the set $(R_0')^{m_0^*}$, consisting of points that return to B_1 under some positive power of $F^{m_0^*}$; this has full measure in B_1. Then consider the corresponding set of returns $\left(\hat{R}_0'\right)^{m_0^*}$. Each point $y_1 \in \left(\hat{R}_0'\right)^{m_0^*}$ is of the form

$$y_1 = F^{m_0} \circ \sigma_{i(0)} \circ F^{n_0}(y_0) \tag{3.1}$$

for some $y_0 \in \Sigma_0$, $n_0 \geq n^*$ and $m_0 \geq m_0^* + k_0$. Denote by Σ_1 the set of points $y_0 \in \Sigma_0$ which correspond, via (3.1), to some point $y_1 \in \hat{R}_1^{m_0^*}$. We obviously have $\Sigma_1 \subseteq \Sigma_0$, and that Σ_1 has positive measure in B_0.

Assume that at the j-th step we have constructed a subset $R_j \subseteq B_j$ which has full measure in B_j, and such that each point $y_j \in R_j$ is of the form

$$y_j = F^{m_{j-1}} \circ \sigma_{i(j-1)} \circ F^{n_{j-1}} \circ \ldots \circ F^{m_0} \circ \sigma_{i(0)} \circ F^{n_0}(y_0), \tag{3.2}$$

some $y_0 \in \Sigma_0$, with $n_0 \geq n^*, \ldots, n_{j-1} \geq n^*$, where n^* is as in Lemma 3.1, depending only on ε, and $m_0 \geq m_0^* + k_0, \ldots, m_{j-1} \geq m_{j-1}^* + k_{j-1}$, where m_{j-1}^* is as in Lemma 3.1, depending on ε, $n_0, \ldots, n_{j-1}, m_0, \ldots, m_{j-2}$. Let Σ_j the set of points $y_0 \in \Sigma_0$ for which the corresponding y_j given by (3.2) is in R_j; we assume that $\Sigma_j \subseteq \Sigma_{j-1} \subseteq \ldots \subseteq \Sigma_0$ has positive measure in B_0.

For the induction step, consider the sets $R^{n^*} \subseteq B_j$ and $\hat{R}^{n^*} \subseteq B_j$, which have full measure in B_j. Let $n_j = n^*$ depending on ε, and m_j^* depending on ε and on $n_0, \ldots, n_j, m_0, \ldots, m_{j-1}$, as in Lemma 3.1. Applying the scattering map $\sigma_{i(j)}$ and then the iterate F^{k_j} to $\hat{R}^{n^*} \subseteq B_j$ yields $(F^{k_j} \circ \sigma_{i(j)})(R_j)$ which has the same measure as B_j. Hence the set $R_j' := [(F^{k_j} \circ \sigma_{i(j)})(R_j)] \cap B_{j+1}$ has full measure in B_{j+1}. The preliminary remarks at the beginning of the proof imply that the corresponding sets $(R_j')^{m_j^*}$ and $(\hat{R}_j')^{m_j^*}$ have full measure in B_{j+1}. Each point $y_{j+1} \in (\hat{R}_j')^{m_j^*}$ is of the form

$$y_{j+1} = F^{m_j} \circ \sigma_{i(j)} \circ F^{n_j}(y_j), \tag{3.3}$$

for some $y_j \in R_j$, where $n_j \geq n^*$ and $m_j \geq m_j^* + k_j$. Let $R_{j+1} := (\hat{R}_j')^{m_j^*}$. Since each $y_j \in R_j$ is of the form (3.2), for some $y_0 \in \Sigma_j$, then each $y_{j+1} \in (\hat{R}_j')^{m_j^*}$ corresponds to some y_0 in some subset $\Sigma_{j+1} \subseteq \Sigma_j$, which has positive measure in B_0. This completes the induction step.

Our construction process involves N steps. At the end of the N-th step we obtain a tower of sets $\Sigma_0 \supseteq \Sigma_1 \supseteq \cdots \supseteq \Sigma_N$, such that each set Σ_j, $j = 0, \ldots, N$, has positive measure in B_0. We also obtain pseudo-orbits of the form $y_0, y_1, \ldots, y_{N-1}, y_N$, with $y_0 \in \Sigma_N$ and

$$y_{j+1} = F^{m_j} \circ \sigma_{i(j)} \circ F^{n_j}(y_j), \tag{3.4}$$

where n_j, m_j are as in Lemma 3.1, for $j = 0, \ldots, N-1$. There is a positive set Σ_N of points y_0 that determine pseudo-orbits as in (3.4).

By construction, each point y_j is inside $B_{\delta_j}(I_j, \phi_j)$. Hence each point $y_j \in B_{\delta_j}(I_j, \phi_j)$ lies at a distance at most $\delta_j < \delta/2 = \varepsilon$ from the level set $\mathcal{L}_{I_j}^{\Sigma}$.

Applying Lemma 3.1 for the pseudo-orbit $\{y_j\}_{j=0,\ldots,N}$ and for the above $\varepsilon > 0$, yields an orbit $\{z_j\}_{j=0,\ldots,N}$ of F with $z_{j+1} = F^{m_j+n_j}(z_j)$, such that $d(z_j, y_j) < \varepsilon$. Since $d(y_j, \mathcal{L}_{I_j}^{\Sigma}) < \varepsilon$ and $\varepsilon = \delta/2$, we conclude $d(z_j, \mathcal{L}_{I_j}^{\Sigma}) < \delta$ for all j.

Then the existence of a trajectory $\Phi^t(z)$ of the flow that visits the δ-neighborhoods of the level sets $\mathcal{L}_{I_j}^{\Sigma}$ in the prescribed order follows immediately. □

4. Numerical verification of the existence of diffusing orbits

4.1. **Computation of geometric objects near the libration point.** We focus on the dynamics near the equilibrium point L_1. We will compute the main geometric object near L_1 that organizes the dynamics. More precisely, we will compute with

high accuracy, using a normal form procedure, the normally hyperbolic invariant manifold near L_1 for a fixed energy level, and its local stable and unstable invariant manifolds. Then, by numerical integration, we will compute the global stable and unstable manifolds.

4.1.1. *Normal form about L_1.* We apply a normal form procedure to simplify the Taylor expansion of the Hamiltonian around the equilibrium point using canonical, near-identity changes of variables. This procedure is carried up to a given (finite) degree in the expansion.

We compute a normal form expansion that is as simple as possible, i.e. one that has the minimum number of monomials. This is usually called a Birkhoff or full normal form. The (truncated) normal form equations can be integrated exactly. As a result, *locally* the normal form gives a very accurate and complete approximation to the dynamics. In a previous paper [22] we have used the same (full) normal form expansion for a different system (Hill's problem).

In particular, we use the action-angle normal form coordinates to parameterize the normally hyperbolic invariant manifold around L_1. We will be particularly interested in the out-of-plane amplitude of motions relative to the ecliptic, which is described via one of the action coordinates later denoted I_v (see Remark 4.10).

Remark 4.1. In contrast, many recent papers [37, 38, 34, 35, 44] use a *partial* normal form procedure known as the "reduction to center manifold". The (truncated) partial normal form equations can *not* be integrated exactly. Still, one can identify some relevant dynamical structures directly from the partial normal form, such as the center manifold or the normally hyperbolic invariant manifold. The main advantage of a partial normal form procedure is that it avoids some small divisors, and thus the normal form is accurate in a larger neighborhood of the equilibrium. For instance, it captures the appearance of periodic 'halo' orbits at a (large) distance of the equilibrium. In this paper we only deal with local diffusion, so we have preferred full normal forms to partial normal forms.

The normal form construction proceeds in three steps. First we perform some convenient translation and scaling of coordinates, and expand the Hamiltonian around L_1 as a power series. Then we make a linear change of coordinates to put the quadratic part of the Hamiltonian in a simple form, which diagonalizes the linear part of the equations of motion. Finally we use the so-called Lie series method to perform a sequence of canonical, near-identity transformations that simplify nonlinear terms in the Hamiltonian of successively higher degree.

4.1.2. *Hamiltonian expansion.* We start by writing the Hamiltonian (2.2) as a power series expansion around the equilibrium point L_1. First we translate the origin of coordinates to the equilibrium point. The distance γ from L_1 to its closest primary (the Earth) is given by the only positive solution of the equation

$$\gamma^5 - (3-\mu)\gamma^4 + (3-2\mu)\gamma^3 - \mu\gamma^2 + 2\mu\gamma - \mu = 0.$$

(See Szebehely [58], section 4.4.)

In order to have good numerical properties for the Taylor coefficients, it is also convenient to scale coordinates [53]. The translation and scaling are given by

$$X = -\gamma x + \mu - 1 + \gamma, \quad Y = -\gamma y, \quad Z = \gamma z. \tag{4.1}$$

Accordingly, the position of the Sun and the Earth are now $P_1 = \left(\frac{1-\gamma}{\gamma}, 0, 0\right)$ respectively $P_2 = (-1, 0, 0)$. The unit of distance is redefined as the distance from the equilibrium point to its closest primary. Since scalings are not canonical transformations, we apply this change of coordinates to the equations of motion, to obtain

$$\ddot{x} - 2\dot{y} = \Omega_x \tag{4.2a}$$

$$\ddot{y} + 2\dot{x} = \Omega_y \tag{4.2b}$$

$$\ddot{z} = \Omega_z, \tag{4.2c}$$

where

$$\Omega = \frac{1}{2}(x^2 + y^2) - \frac{\mu - 1 + \gamma}{\gamma}x + \frac{1}{\gamma^3}\left(\frac{1-\mu}{r_1} + \frac{\mu}{r_2}\right)$$

and r_1, r_2 denote the (scaled) distances from the third body to the larger and the smaller primary, respectively:

$$r_1^2 = \left(x - \frac{\gamma - 1}{\gamma}\right)^2 + y^2 + z^2$$
$$r_2^2 = (x-1)^2 + y^2 + z^2.$$

Defining $p_x = \dot{x} - y$, $p_y = \dot{y} + x$, $p_z = \dot{z}$, the libration-point centered equations of motion (4.2) are Hamiltonian, with Hamiltonian function

$$H = \frac{1}{2}(p_x^2 + p_y^2 + p_z^2) + yp_x - xp_y + \frac{\mu - 1 + \gamma}{\gamma}x - \frac{1}{\gamma^3}\left(\frac{1-\mu}{r_1} + \frac{\mu}{r_2}\right). \tag{4.3}$$

We use Legendre polynomials to expand the nonlinear terms in the Hamiltonian (4.3) according to the formula

$$\frac{1}{\sqrt{(x-A)^2 + (y-B)^2 + (z-C)^2}} = \frac{1}{D}\sum_{n=0}^{\infty}\left(\frac{\rho}{D}\right)^n P_n\left(\frac{Ax + By + Cz}{D\rho}\right), \tag{4.4}$$

where $D^2 = A^2 + B^2 + C^2$, $\rho^2 = x^2 + y^2 + z^2$, and P_n is the nth Legendre polynomial. This expansion holds where $\rho < D$.

The Hamiltonian is then rewritten in the form

$$H = \frac{1}{2}(p_x^2 + p_y^2 + p_z^2) + yp_x - xp_y - \sum_{n\geq 2} c_n(\mu)\rho^n P_n\left(\frac{x}{\rho}\right), \tag{4.5}$$

where the coefficients $c_n(\mu)$ are given by

$$c_n(\mu) = \frac{1}{\gamma^3}\left(\mu + (-1)^n\frac{(1-\mu)\gamma^{n+1}}{(1-\gamma)^{n+1}}\right).$$

This expansion holds where $\rho < \min(|P_1|, |P_2|) = |P_2| = 1$, i.e. it is valid in a ball centered at L_1 that extends up to the Earth.

Notice that the constants c_n have the desirable property that they are all of the same order of magnitude. (This property is due to the scaling (4.1).) Thus the effect of high-order terms in the Hamiltonian expansion (4.5) is basically measured by the factor ρ^n.

Richardson [53] initially developed the equations into this form, which is well-suited for use in perturbative methods such as normal forms, where one needs to assess the relative importance of various orders of magnitude in the perturbing

function. It also allows computation of high-order terms using simple recursive relationships.

4.1.3. *Linear preliminaries.* Now we transform the *linear* part of the system into Jordan form, which is convenient for the normal form procedure. This particular transformation is derived in [37, 38], for instance.

Consider the quadratic part H_2 of the Hamiltonian (4.5),

$$H_2 = \frac{1}{2}(p_x^2 + p_y^2 + p_z^2) + yp_x - xp_y - c_2x^2 + \frac{c_2}{2}y^2 + \frac{c_2}{2}z^2, \tag{4.6}$$

which corresponds to the linearization of the equations of motion. It is well-known [38] that the linearized system has eigenvalues of the form $\pm\lambda, \pm i\nu, \pm i\omega$, where λ, ν, ω are real and positive.

One can find ([38] section 2.1) a symplectic linear change of variables χ from position-momenta to new variables $(x, y) = (x_1, y_1, x_2, y_2, x_3, y_3) \in \mathbb{R}^6$,

$$(x, y, z, p_x, p_y, p_z) = \chi(x_1, y_1, x_2, y_2, x_3, y_3), \tag{4.7}$$

that casts the quadratic part of the Hamiltonian into

$$H_2 = \lambda x_1 y_1 + \frac{\nu}{2}(x_2^2 + y_2^2) + \frac{\omega}{2}(x_3^2 + y_3^2). \tag{4.8}$$

The linear equations of motion $(\dot{x}, \dot{y}) = A(x, y)$ associated to (4.8) decouple into a hyperbolic and a center part

$$(\dot{x}_1, \dot{y}_1) = A_h(x_1, y_1) \tag{4.9a}$$

$$(\dot{x}_2, \dot{y}_2, \dot{x}_3, \dot{y}_3) = A_c(x_2, y_2, x_3, y_3), \tag{4.9b}$$

with

$$A_h = \begin{pmatrix} \lambda & 0 \\ 0 & -\lambda \end{pmatrix} \qquad \text{and} \qquad A_c = \begin{pmatrix} 0 & \nu & & \\ -\nu & 0 & & \\ & & 0 & \omega \\ & & -\omega & 0 \end{pmatrix}.$$

Remark 4.2. The solution of these linear equations is

$$\begin{aligned} x_1(t) = x_1^0 e^{\lambda t}, \quad y_1(t) = y_1^0 e^{-\lambda t} \\ x_2(t) + iy_2(t) = (x_2^0 + iy_2^0)e^{-i\nu t} \\ x_3(t) + iy_3(t) = (x_3^0 + iy_3^0)e^{-i\omega t}, \end{aligned}$$

where (x_i^0, y_i^0) are initial conditions. Thus the solution is composed of three uncoupled motions: a saddle in the (x_1, y_1) coordinates, and two harmonic oscillators in the (x_2, y_2) and (x_3, y_3) coordinates.

Remark 4.3. Due to the particular form of the change of coordinates C, the pair (x_3, y_3) is just a rescaling of the SCRTBP coordinates (z, p_z), so the (x_3, y_3) oscillation is perpendicular to the xy plane of motion of the primaries, whereas the (x_2, y_2) oscillation happens on the xy plane. Thus they are sometimes called the "out-of-plane" and the "in-plane" oscillation respectively.

Notice that the matrix A of the linear equations (4.9) is in block-diagonal form. It is convenient to diagonalize the matrix A over $\mathbb{C}$ so that the homological operator

(definition 4.14) takes a specially simple form. Consider the *symplectic* change $T^{-1}\colon \mathbb{R}^6 \to \mathbb{C}^6$ to complex variables $(q,p) = (q_1,p_1,q_2,p_2,q_3,p_3) \in \mathbb{C}^6$

$$q_1 = x_1, \quad p_1 = y_1 \tag{4.11a}$$

$$q_2 = \frac{1}{\sqrt{2}}(x_2 - iy_2), \quad p_2 = \frac{1}{\sqrt{2}}(-ix_2 + y_2) \tag{4.11b}$$

$$q_3 = \frac{1}{\sqrt{2}}(x_3 - iy_3), \quad p_3 = \frac{1}{\sqrt{2}}(-ix_3 + y_3). \tag{4.11c}$$

This change casts the quadratic part of the Hamiltonian into

$$H_2 = \lambda q_1 p_1 + i\nu q_2 p_2 + i\omega q_3 p_3. \tag{4.12}$$

Equivalently, this change carries A to diagonal form:

$$T^{-1}AT = \Lambda = \operatorname{diag}(\lambda, -\lambda, i\nu, -i\nu, i\omega, -i\omega).$$

Remark 4.4. Below we consider the real system $H(x,y)$ that has been transformed to a complex system, say $K(q,p)$, to simplify the computation of the normal form. Notice that H can be thought of as being defined on $(x,y) \in \mathbb{C}^6$ but taking real values when $(x,y) \in \mathbb{R}^6$. After complexification, $K(q,p) = \sum k_{\alpha\beta} q^\alpha p^\beta$ is defined on $(q,p) \in \mathbb{C}^6$ but must take real values when $(q_1,p_1) \in \mathbb{R}^2$ and $\bar{p}_j = iq_j$ for $j = 2,3$. Thus we have the following *reality conditions* on the coefficients $k_{\alpha\beta}$:

$$k_{\alpha_1\alpha_2\alpha_3\beta_1\beta_2\beta_3} = i^{\alpha_2+\alpha_3+\beta_2+\beta_3} \bar{k}_{\alpha_1\beta_2\beta_3\beta_1\alpha_2\alpha_3}. \tag{4.13}$$

Remark 4.5. Below we compute the normal form in complex variables. The inverse change of (4.11) carries this complex normal form back to a real normal form (with respect to (4.9)). The fact that the final series is real follows from the preservation of the reality conditions by the normalization transformations. Also, the final change of variables that brings the system to normal form is real.

4.1.4. *Normal form.* Assume that the symplectic linear changes of variables (4.7) and (4.11) have been performed in the Hamiltonian expansion (4.5), so that the quadratic part H_2 is already in the form (4.12).

Let us then write the Hamiltonian as

$$H(q,p) = H_2(q,p) + H_3(q,p) + H_4(q,p) + \cdots \tag{4.14}$$

with $H_j(q,p)$ a homogeneous polynomial of degree j in the variables $(q,p) \in \mathbb{C}^6$.

Next we remove most monomials in the series (4.14) by means of a formal sequence of coordinate transformations, in order to obtain an integrable approximation to the dynamics close to the equilibrium point.

Theorem 4.6 (Birkhoff normal form around a saddle × centre × centre)**.** *For any integer $N \geq 3$, there exists a neighborhood $\mathcal{U}^{(N)}$ of the origin and a near-identity canonical transformation $\mathcal{T}^{(N)}\colon\ \mathbb{C}^6 \supset \mathcal{U}^{(N)} \mapsto \mathbb{C}^6$ that puts the system* (4.14) *in normal form up to order N, namely*

$$\mathcal{H}^{(N)} := H \circ \mathcal{T}^{(N)} = H_2 + \mathcal{Z}^{(N)} + \mathcal{R}^{(N)}$$

where $\mathcal{Z}^{(N)}$ is a polynomial of degree N that Poisson-commutes with H_2

$$\{\mathcal{Z}^{(N)}, H_2\} \equiv 0,$$

and $\mathcal{R}^{(N)}$ is small

$$|\mathcal{R}^{(N)}(z)| \leq C_N ||z||^{N+1} \quad \forall z \in \mathcal{U}^{(N)}.$$

If the elliptic frequencies ν, ω are nonresonant to degree N,

$$c_1\nu + c_2\omega \neq 0 \qquad \forall (c_1, c_2) \in \mathbb{Z}^2, \quad 0 < |c_1 + c_2| \leq N,$$

then in the new coordinates, the truncated Hamiltonian $H_2 + \mathcal{Z}^{(N)}$ depends only on the basic invariants

$$I_h = q_1 p_1 = x_1 y_1 \tag{4.15a}$$

$$I_p = i q_2 p_2 = q_2 \bar{q}_2 = \frac{x_2^2 + y_2^2}{2} \tag{4.15b}$$

$$I_v = i q_3 p_3 = q_3 \bar{q}_3 = \frac{x_3^2 + y_3^2}{2}. \tag{4.15c}$$

Remark 4.7. The equations of motion associated to the *truncated normal form* $H_2 + \mathcal{Z}^{(N)}$ can be integrated exactly. Using (4.8), the truncated normal form can be written in terms of the new coordinates as

$$H_2 + \mathcal{Z}^{(N)} = \lambda I_h + \nu I_p + \omega I_v + \mathcal{Z}^{(N)}(I_h, I_p, I_v).$$

Remark 4.8. The reminder $\mathcal{R}^{(N)}$ is very small in a small neighborhood of the origin. Hence, close to the origin, the exact solution of the truncated normal form is a very accurate approximate solution of the original system H.

Remark 4.9. Let ϕ_h, ϕ_p, ϕ_v be the symplectic conjugate variables to I_h, I_p, I_v, respectively. The variables (I_h, ϕ_h) correspond to the hyperbolic component of the dynamics. The normally hyperbolic invariant manifold near L_1 corresponds to $I_h = 0$. The basic invariants I_p and I_v are usually called *action variables*, and their conjugate variables ϕ_p, ϕ_v are usually called *angle variables*. They are given in polar variables (ρ, ϕ) by $I_p = \frac{\rho_2^2}{2}$ and $I_v = \frac{\rho_3^2}{2}$, where $\rho_2^2 = x_2^2 + y_2^2$ and $\rho_3^2 = x_3^2 + y_2^3$

Remark 4.10. To make the notation more intuitive, we have named the second action-angle pair (I_p, ϕ_p), where the subscript p suggests the 'planar component', and the third action-angle pair (I_v, ϕ_v), where the subscript v suggests the 'vertical component'. Notice that the new coordinates (4.15) are related to the old linear coordinates (4.8) by a near-identity transformation. Thus, in the linear aproximation, I_p represents the *in-plane* action, and I_v represents the *out-of-plane* action, as explained in Remark 4.3.

Remark 4.11. In practice, we compute a normal form of degree $N = 16$. See some comments in Remark 4.21.

In the rest of this section, we give a proof of Theorem 4.6. The proof consists of an algorithm to find the transformation $\mathcal{T}^{(N)}$ that puts the original system in normal form.

There are several normal form algorithms in the litterature. (The book by Murdock [50] studies different algorithms, or "formats", in a general setting.) We use the so-called *Lie series method* [37], or "generated iterative format", because it is well-suited to Hamiltonian systems and it is computationally very efficient.

Definition 4.12. Let $\mathbb{H}_j$ be the vector space of homogeneous polynomials of degree j in the variables $(q, p) \in \mathbb{C}^6$.

Let $\{H, K\}$ be the *Poisson bracket* of two functions, given by

$$\{H, K\} = \sum_{i=1}^{3} \left(\frac{\partial H}{\partial q_i} \frac{\partial K}{\partial p_i} - \frac{\partial H}{\partial p_i} \frac{\partial K}{\partial q_i} \right).$$

Remark 4.13. If $H \in \mathbb{H}_i$ and $K \in \mathbb{H}_j$ then $\{H, K\} \in \mathbb{H}_{i+j-2}$.

In the Lie series method, we look for a sequence of canonical coordinate transformations

$$\mathcal{T}^{(N)} := \Phi_N \circ \Phi_{N-1} \circ \Phi_{N-2} \circ \cdots \circ \Phi_3$$

to be applied to the Hamiltonian $H(q,p)$. The crucial idea is to use as each basic canonical coordinate transformation Φ_j the *time-one flow* of a Hamiltonian $G_j \in \mathbb{H}_j$ for $j = 3, 4, 5, \ldots$. We recall that the time-t flow of a Hamiltonian system is always a canonical transformation. The Hamiltonian G_j is called the *generating Hamiltonian* of the transformation.

It is not hard to see that the coordinate transformation Φ_j acts formally on the Hamiltonian H in the following way:

$$\begin{aligned} K &\equiv H \circ \Phi_j \\ &= H + \{H, G_j\} + \frac{1}{2!}\{\{H, G_j\}, G_j\} + \frac{1}{3!}\{\{\{H, G_j\}, G_j\}, G_j\} + \cdots . \end{aligned} \tag{4.16}$$

Notice that the action of the transformation on the Hamiltonian H is completely determined by its generating Hamiltonian G_j. The new Hamiltonian will temporarily be called

$$K = K_2 + K_3 + K_4 + \cdots ,$$

with $K_i \in \mathbb{H}_i$.

Since $G_j \in \mathbb{H}_j$ is assumed to be a homogeneous polynomial of degree j, the action of the transformation (4.16) leaves terms $K_i = H_i$ of lower degree $i < j$ unmodified. Terms of degree j are modified according to

$$K_j = H_j + \{H_2, G_j\}. \tag{4.17}$$

Terms K_i of higher degree $i > j$ are also modified by the transformation.

The normal form algorithm is an iterative procedure. Every iteration is as follows:

- Begin with a Hamiltonian $H(q,p)$ in the form (4.14), assuming it to be normalized to degree $j-1$, i.e. assuming that $H_2, H_3, \ldots, H_{j-1}$ are in "normal form" (to be made precise in definition 4.17).
- Perform one normalization step to put the j-th degree terms in normal form. In the light of equation (4.17), we need to choose a generating Hamiltonian G_j such that K_j becomes as simple as possible.
- Compute the rest of K (i.e. K_i for $i > j$) from expression (4.16). Then K is renamed H, and the process is iterated for the next j.

Definition 4.14. Let $\mathcal{L}_j \colon \mathbb{H}_j \to \mathbb{H}_j$ be the *homological operator*, defined as

$$\mathcal{L}_j = \mathcal{L}_{H_2} = \{\cdot, H_2\}.$$

The heart of the process is the normalization step, where G_j is chosen such that $K_j = H_j + \{H_2, G_j\}$ becomes as simple as possible. Thus we are led to study the *homological equation*

$$\mathcal{L}_j G_j = H_j - K_j. \tag{4.18}$$

Ideally, one would like to make $K_j = 0$. This can be accomplished whenever $H_j \in \mathrm{im}\mathcal{L}_j$. In general (depending on H_2), $\mathrm{im}\mathcal{L}_j \neq \mathbb{H}_j$ so one can not make $K_j = 0$. However, if $\mathbb{N}_j$ is a complement to $\mathrm{im}\mathcal{L}_j$ in the space $\mathbb{H}_j$,

$$\mathbb{H}_j = \mathrm{im}\mathcal{L}_j \oplus \mathbb{N}_j,$$

we can certainly make K_j lie in the complement $\mathbb{N}_j$.

Of course, the aim is to have a "simple" complement $\mathbb{N}_j$, so that the only j-th degree terms left $K_j \in \mathbb{N}_j$ do not prevent integrability of the resulting Hamiltonian.

Next we describe the complement $\mathbb{N}_j$ when the quadratic part of the Hamiltonian H_2 has the form (4.12). It is useful to introduce multi-index notation.

Definition 4.15. If $k = (k_1, k_2, \dots, k_n) \in \mathbb{N}^n$ is a vector of non-negative numbers, then define

$$x^k = x_1^{k_1} x_2^{k_2} \cdots x_n^{k_n},$$

a monomial of degree

$$|k| = k_1 + k_2 + \cdots + k_n.$$

Proposition 4.16. *If $H_2 = \lambda q_1 p_1 + i\nu q_2 p_2 + i\omega q_3 p_3$, then the homological operator $\mathcal{L}_j \colon \mathbb{H}_j \to \mathbb{H}_j$ defined as $\mathcal{L}_j = \mathcal{L}_{H_2} = \{\cdot, H_2\}$ is semisimple for each j.*

Proof. Let $q^l p^m$ be a monomial of degree $j = |l + m|$. An easy calculation shows that

$$\mathcal{L}_j q^l p^m = < l - m, \bar{\lambda} > q^l p^m,$$

where

$$\bar{\lambda} = (\lambda, i\nu, i\omega)$$

and

$$< l - m, \bar{\lambda} > = (l_1 - m_1)\lambda + i(l_2 - m_2)\nu + i(l_3 - m_3)\omega.$$

Hence, the standard basis for $\mathbb{H}_j$ consists of eigenvectors of $\mathcal{L}_j$, which is therefore semisimple. Specifically, the eigenvalues of $\mathcal{L}_j$ are $< l-m, \bar{\lambda} >$ with $|l+m| = j$. □

Since the homological operator is semisimple, it follows that $\mathbb{H}_j = \mathrm{im}\mathcal{L}_j \oplus \ker \mathcal{L}_j$ (Murdock [50], Theorem 2.1.3). Therefore, we can choose as complement subspace

$$\mathbb{N}_j = \ker \mathcal{L}_j.$$

Definition 4.17. We say that a formal power series Hamiltonian $H(q,p) = H_2(q,p) + H_3(q,p) + \cdots$ is in *normal form* with respect to $H_2 = \lambda q_1 p_1 + i\nu q_2 p_2 + i\omega q_3 p_3$ to degree N if

$$H_j \in \mathbb{N}_j = \ker \mathcal{L}_j \qquad \text{for } j = 3, 4, \dots, N$$

or equivalently, if H_j commutes with the quadratic part H_2.

The iterative procedure outlined above describes how to transform the original Hamiltonian (4.14) to its normal form. In practice, we only compute the normal form to finite degree N.

Corollary 4.18. *The space $\ker \mathcal{L}_j$ is spanned as a vector space over $\mathbb{C}$ by the monomials $q^l p^m \in \mathbb{H}_j$ such that*

$$< l - m, \bar{\lambda} > = 0,$$

or equivalently such that the following relations hold simultaneously:

$$l_1 - m_1 = 0 \qquad \text{and} \tag{4.19a}$$

$$(l_2 - m_2)\nu + (l_3 - m_3)\omega = 0. \tag{4.19b}$$

The structure of the normal form space $\mathbb{N}_j = \ker \mathcal{L}_j$ depends on the relation between the frequencies ν and ω, whether they are resonant or not. Since we are only interested on finite degree normal forms, it is enough to ask for a non-resonance condition to degree N.

Definition 4.19. The frequencies ν and ω are *non-resonant to degree* N if

$$c_1\nu + c_2\omega \neq 0 \qquad \forall (c_1, c_2) \in \mathbb{Z}^2, \quad 0 < |c_1 + c_2| \leq N.$$

Suppose that the frequencies are non-resonant to degree N. (In practice, this assumption has to be verified numerically for the actual values of ν and ω, but it is a finite computation.) Then the only solutions to equation (4.19b) have $l_2 = m_2$ and $l_3 = m_3$, for $0 < |l_2 - m_2 + l_3 - m_3| \leq N$. Hence the normal form space $\mathbb{N}_j$ is spanned over $\mathbb{C}$ by monomials of the form

$$q^l p^l = (q_1 p_1)^{l_1} (q_2 p_2)^{l_2} (q_3 p_3)^{l_3},$$

of degree $j = 2|l|$, for $3 \leq j \leq N$.

Remark 4.20. In particular, $\mathbb{N}_j = \emptyset$ whenever j is odd.

Note that these monomials do not satisfy the reality condition (4.13). However, the normal form space is spanned over $\mathbb{R}$ by monomials of the form

$$(q_1 p_1)^{l_1} (i q_2 p_2)^{l_2} (i q_3 p_3)^{l_3},$$

of degree $j = 2|l|$. We express the normal form in terms of this real basis.

Therefore, if the elliptic frequencies are non-resonant to degree N, the normal form space is spanned by monomials of the form $I_h^{l_1} I_p^{l_2} I_v^{l_3}$. This concludes the proof of Theorem 4.6.

Remark 4.21. Numerically, it is convenient to avoid small divisors when solving for G_j in the normalization step. Thus, in our computations, we check that there are no *quasi-resonances* up to degree N, i.e. we check that

$$|c_1\nu + c_2\omega| \geq \varepsilon \qquad \forall (c_1, c_2) \in \mathbb{Z}^2, \quad 0 < |c_1 + c_2| \leq N.$$

In particular, for $N = 16$ we find that ε can be taken as large as 0.1.

Therefore, we can apply Theorem 4.6 to the Hamiltonian of the SCRTBP expanded around the equilibrium point L_1. Using the iterative procedure outlined above, we compute the normal form $\mathcal{H}^{(N)}$ to degree $N = 16$.

4.2. **Computation of the Stable and Unstable Manifolds.** For the rest of the paper, we assume that the energy condition (2.3) is fixed to any value c with

$$c_{halo} < c < c_1,$$

where $c_1 := C(L_1) \approx 3.00088\cdots$ is the Jacobi constant of the equilibrium point L_1, and $c_{halo} := C(halo) \approx 3.00082\cdots$ is the critical value at which the so-called *halo orbits* appear. Thus the motion in the center manifold of L_1 restricted to this energy value is essentially quasi-periodic (see Gómez *et al* [35]).

Consider the truncated normal form

$$\mathcal{H}^{(N)}_{\text{trunc}} := H_2 + \mathcal{Z}^{(N)}$$

of the SCRTBP around the equilibrium point L_1. Let x_1, y_1 be the hyperbolic normal form coordinates (4.15a). It is not hard to see that the 4-dimensional manifold

(4.20)

$$W^{c,(N)}(L_1) := \{(x_1, y_1, I_p, \phi_p, I_v, \phi_v) \colon\ x_1 = y_1 = 0,\ I_p, I_v \in \mathbb{R}^+,\ \phi_p, \phi_v \in \mathbb{T}\}.$$

is the invariant center manifold for $\mathcal{H}^{(N)}_{\text{trunc}}$.

Also the 3-dimensional manifold

$$\Lambda_c^{(N)} := W^{c,(N)}(L_1) \cap M = \{(I_p, \phi_p, I_v, \phi_v) \in W^{c,(N)}(L_1) \colon\ C(I_p, I_v) = c\} \tag{4.21}$$

is a normally hyperbolic invariant manifold for $\mathcal{H}^{(N)}_{\text{trunc}}$. The manifold Λ_c can be parameterized by (I_p, ϕ_p, ϕ_v) or (I_v, ϕ_p, ϕ_v) (the actions are related by the energy condition $C(I_p, I_v) = c$). We choose to use the action I_v to parameterize it.

Let us clarify the relation between the invariant objects in the original system and in the truncated system. The center manifold in the original system and the center manifold in the truncated system are C^N-close in the following sense: For each integer r with $N \leq r < \infty$, there exists a (not necessarily unique) local invariant center manifold $W^c(L_1)$ of the original system, which is of class C^r and is expressible as a graph over $W^{c,(N)}(L_1)$, and having Nth order contact with $W^{c,(N)}(L_1)$. (See Murdock [50], chapter 5.)

We *assume* that, for the range of energy values considered, there exists a NHIM of class C^r in the original system, diffeomorphic to S^3. Since it is compact, it must be unique, as explained in Section 2.2. The NHIM in the original system and the NHIM in the truncated system are also C^N-close, since they are contained in the center manifold.

We do *not* need to assume the existence of invariant tori in the original system. Instead, we consider 2-dimensional level sets $\mathcal{L}_{\bar{I}} = \{I_v = \bar{I}\} \cap \Lambda_c$ of the out-of-plane action I_v, which correspond to invariant tori

$$T_{\bar{I}} := \{(I_v, \phi_p, \phi_v) \in \Lambda \colon\quad I_v = \bar{I}\} \tag{4.22}$$

in the normal form approximation. Each torus $T_{\bar{I}}$ is invariant under the flow corresponding to the truncated Hamiltonian $\mathcal{H}^{(N)}$ given by Theorem 4.6. Each corresponding level set is the image of such a torus via the normal form transformation $\mathcal{T}^{(N)}$, i.e.,

$$\mathcal{L}_{\bar{I}} = \mathcal{T}^{(N)}\left(T_{\bar{I}}\right).$$

The action level set $\mathcal{L}_{\bar{I}}$ is geometrically a 2-dimensional torus, but it it not invariant by the original flow, only 'approximately invariant'.

Numerically, we use the parametrizations (4.20), (4.21) and (4.22) to represent the manifolds $W^c(L_1)$, Λ_c and $\mathcal{L}_{\bar{I}}$. We simply discretize the variables I_p, I_v, ϕ_p, ϕ_v into a finite grid of points, and transform the resulting grid to original coordinates by the normal form transformation. Indeed, the objects in the truncated system can be thought of as model manifolds for the objects in the original system. As discussed above, those numerical approximations are close to the true invariant objects. Thus, from a numerical standpoint we do not make any distinction between $T_{\bar{I}}$ and $\mathcal{L}_{\bar{I}}$.

Remark 4.22. Close to the equilibrium point, one can use either normal form or original coordinates to parametrize the manifolds. In practice, we transform coordinates from and to normal form as needed using $\mathcal{T}^{(N)}$ and its inverse $\left(\mathcal{T}^{(N)}\right)^{-1}$. In our notation, we do not distinguish between manifolds written in normal form and original coordinates.

Note that Λ_c is a compact manifold which consists of a 1-parameter family of action level sets:

$$\Lambda_c = \bigcup_{\bar{I} \in [0, I_{\max}]} \mathcal{L}_{\bar{I}}.$$

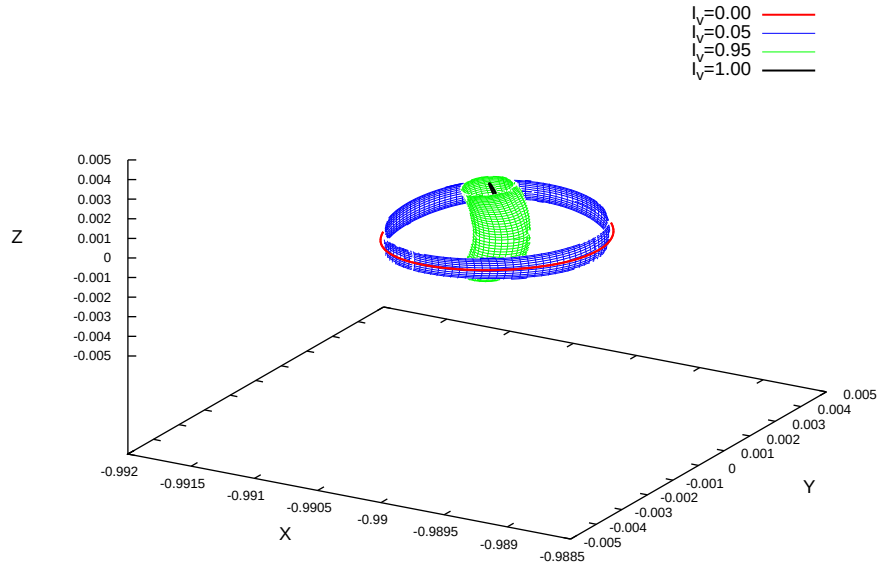

FIGURE 2. The normally hyperbolic invariant manifold Λ_c as a family of invariant tori of increasing out-of-plane action I_v. It is plotted in the original SCRTBP coordinates (2.1). This NHIM corresponds to a low energy $c = 3.00088$. (Refer to the definition of I_v in equation (4.15c). See also Remark 4.10 on the meaning of 'out-of-plane').

Figures 2 and 3 show two NHIM corresponding to two different energies: a low energy $c = 3.00088$ close to c_1, and a high energy $c = 3.00083$ close to c_{halo}. Actually, we only show a few representative level sets in Λ_c.

Remark 4.23. The maximum out-of-plane action $I_{\max}$ depends on the value of the energy considered. For example, $c = 3.00088$ yields a maximum action $I_{\max} \simeq 0.052$, whereas $c = 3.00083$ yields a maximum action $I_{\max} \simeq 0.17$. To compare different energies, in the figures we normalize the out-of-plane action to lie on $[0, 1]$.

All these objects have associated stable and unstable (or *asymptotic*) invariant manifolds of one more dimension than the object itself. The normal form provides a very accurate approximation to the local asymptotic manifolds in a small neighborhood of Λ. Outside this neighborhood, the asymptotic manifolds are globalized using numerical integration.

Let $\Upsilon^s = \Upsilon^u = (0, \upsilon) \subset \mathbb{R}$ be a small interval in the stable (resp. unstable) coordinates. (In practice, we take $\upsilon = 10^{-5}$). The local invariant center-stable and center-unstable manifolds are given by

$$\begin{aligned} W^{cs}_{loc} &:= W^c(L_1) \oplus \Upsilon^s \\ &= \{(x_1, y_1, I_p, \phi_p, I_v, \phi_v) \colon\ x_1 = 0,\ y_1 \in \Upsilon^s, \quad I_p, I_v \in \mathbb{R}^+, \quad \phi_p, \phi_v \in \mathbb{T}\}, \end{aligned}$$

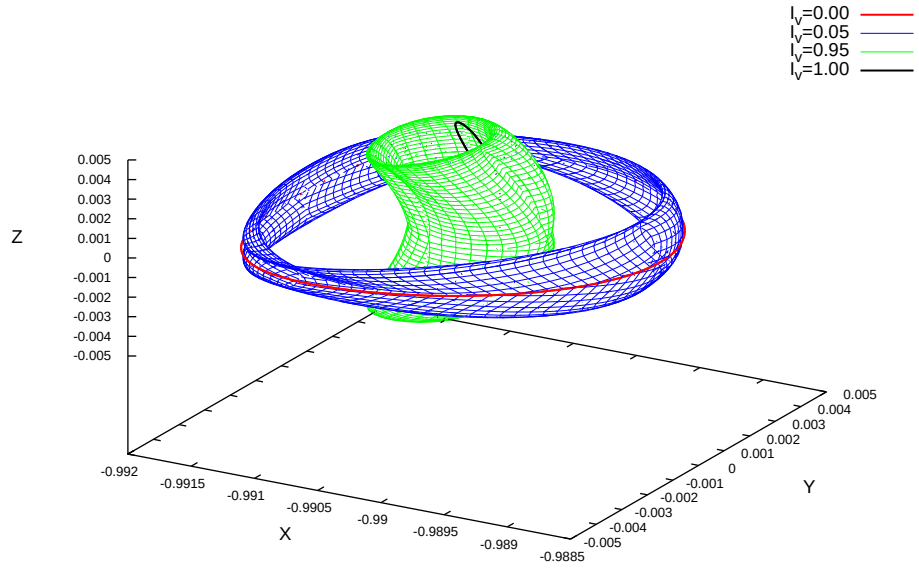

FIGURE 3. This NHIM corresponds to a high energy $c = 3.00083$.

$$W^{cu}_{loc} := W^c(L_1) \oplus \Upsilon^u$$
$$= \{(x_1, y_1, I_p, \phi_p, I_v, \phi_v) \colon\ x_1 \in \Upsilon^u,\ y_1 = 0, \quad I_p, I_v \in \mathbb{R}^+, \quad \phi_p, \phi_v \in \mathbb{T}\}.$$

The 4-dimensional local stable and unstable invariant manifolds of Λ_c are

$$W^s_{loc}(\Lambda_c) := \Lambda_c \oplus \Upsilon^s, \qquad W^u_{loc}(\Lambda_c) := \Lambda_c \oplus \Upsilon^u. \tag{4.23}$$

The 3-dimensional local stable and unstable (non-invariant) manifolds of $\mathcal{L}_I$ are

$$W^s_{loc}(\mathcal{L}_{\bar I}) := \mathcal{L}_{\bar I} \oplus \Upsilon^s, \qquad W^u_{loc}(\mathcal{L}_{\bar I}) := \mathcal{L}_{\bar I} \oplus \Upsilon^u. \tag{4.24}$$

The decomposition of Λ_c into level sets implies an analogous decomposition of the asymptotic manifolds

$$W^s_{loc}(\Lambda_c) = \bigcup_{\bar I \in [0, I_{\max}]} W^s_{loc}(\mathcal{L}_{\bar I}), \qquad W^u_{loc}(\Lambda_c) = \bigcup_{\bar I \in [0, I_{\max}]} W^u_{loc}(\mathcal{L}_{\bar I}).$$

We use this property to compute $W^s_{loc}(\Lambda_c)$, $W^u_{loc}(\Lambda_c)$ numerically: it is enough to compute $W^s_{loc}(\mathcal{L}_{\bar I})$, $W^u_{loc}(\mathcal{L}_{\bar I})$ for a "dense" set of actions $\bar I$.

Recall that the asymptotic manifolds are invariant for the dynamics. To obtain the *global* asymptotic manifolds $W^s(\mathcal{L}_{\bar I})$, $W^u(\mathcal{L}_{\bar I})$, we propagate the local manifolds using numerical integration. More precisely, we do the following:

(1) Fix a 2-dimensional section of the stable manifold at a distance $\upsilon = 10^{-5}$ of the action level set $\mathcal{L}_{\bar I}$ measured along $W^s_{loc}(\mathcal{L}_{\bar I})$, and similarly for the unstable manifold:

$$W^s_\upsilon(\mathcal{L}_{\bar I}) := W^s(\mathcal{L}_{\bar I}) \cap \{y_1 = \upsilon\}, \tag{4.25}$$
$$W^u_\upsilon(\mathcal{L}_{\bar I}) := W^u(\mathcal{L}_{\bar I}) \cap \{x_1 = \upsilon\}. \tag{4.26}$$

These sets belong to the boundary of the local stable (resp. unstable) manifolds of $\mathcal{L}_{\bar{I}}$ as given in (4.24).

(2) Transform the sets $W^s_v(\mathcal{L}_{\bar{I}}), W^u_v(\mathcal{L}_{\bar{I}})$ back to SCRTBP coordinates (2.1).
(3) Consider $W^u_v(\mathcal{L}_{\bar{I}})$ as a set of initial conditions, and integrate the corresponding trajectories forward in time using SCRTBP equations (2.1). The resulting orbits approximate the global unstable manifold.
(4) Consider $W^s_v(\mathcal{L}_{\bar{I}})$ as a set of initial conditions, and integrate the corresponding trajectories backward in time using SCRTBP equations (2.1). The resulting orbits approximate the global stable manifold.

Recall from section 2 that there exists a *preserved fibration* of the stable/unstable manifold $W^{u,s}(\Lambda_c)$ by the stable/unstable manifolds of points on Λ_c

$$W^{s,u}(\Lambda_c) = \bigcup_{x\in\Lambda_c} W^{s,u}(x).$$

Remark 4.24. The stable and unstable fibrations are *not* invariant by the flow. Instead, they are *preserved* by the flow Φ, meaning that fibers are carried into fibers. In other words, if two points x and y belong to the same fiber, then $\Phi^t(x)$ and $\Phi^t(y)$ belong to the same fiber for every t.

Let $z = (\bar{I}, \bar{\phi}_p, \bar{\phi}_v)$ be a point on Λ_c. The local stable and unstable manifolds of z are given by

(4.27)
$$\begin{aligned} W^s_{loc}(z) :=& z \oplus \Upsilon^s \\ =& \{(x_1, y_1, I_p, \phi_p, I_v, \phi_v) \colon\ x_1 = 0,\ y_1 \in \Upsilon^s, \quad I_v = \bar{I}_v,\ C(I_p, I_v) = c, \\ & \phi_p = \bar{\phi}_p,\ \phi_v = \bar{\phi}_v\} \end{aligned}$$

(4.28)
$$\begin{aligned} W^u_{loc}(z) :=& z \oplus \Upsilon^u \\ =& \{(x_1, y_1, I_p, \phi_p, I_v, \phi_v) \colon\ x_1 \in \Upsilon^u,\ y_1 = 0, \quad I_v = \bar{I}_v,\ C(I_p, I_v) = c, \\ & \phi_p = \bar{\phi}_p,\ \phi_v = \bar{\phi}_v\}. \end{aligned}$$

4.3. **Computation of Homoclinic Points.** Next we explain the procedure used to compute the intersection of the stable and unstable manifolds $W^s(\Lambda_c) \cap W^u(\Lambda_c)$ restricted to a suitable surface of section $\mathcal{S}$. Our procedure is similar to the one used by Masdemont [44]. The main difference is that we decompose $W^s(\Lambda_c)$ and $W^u(\Lambda_c)$ into level sets for the purpose of the computation.

The procedure consists of the following three steps:

(1) First integrate the stable and unstable invariant manifolds until they cut the surface of section $\mathcal{S}$ for the first time. This gives rise to two sets of points on the section, denoted $W^s_{\mathcal{S}}(\mathcal{L}_I)$ and $W^u_{\mathcal{S}}(\mathcal{L}_I)$.
(2) Then look for approximate intersections between these two sets. We look for pairs of points (x_1, x_2) with $x_1 \in W^u_{\mathcal{S}}(\mathcal{L}_I)$ and $x_2 \in W^s_{\mathcal{S}}(\mathcal{L}_I)$ such that their distance $|x_1 - x_2|$ in phase space is small.
(3) Finally refine these approximate intersections using a Newton method to obtain true intersections, i.e. zeros of the distance function $|x_1 - x_2|$.

Let us describe these three steps in more detail, and present the numerical results. For the first step, we fix a 5-dimensional surface of section

$$\mathcal{S} = \{(x, y, z, \dot{x}, \dot{y}, \dot{z}) \colon\ y = 0,\ \dot{y} > 0\}.$$

This section corresponds to crossing the xz-plane (with positive y velocity) in synodic SCRTBP coordinates (4.2). Notice that the choice of the section $\mathcal{S}$ is somewhat arbitrary; it is only related to the computation procedure. Specifically, the section is used to reduce the dimension of the manifolds and their intersection. This way, the problem to compute their intersection becomes simpler.

To integrate the asymptotic manifolds, we select initial conditions on the local stable and unstable manifolds of Λ_c at a small distance $\upsilon = 10^{-5}$ of the normally hyperbolic invariant manifold Λ_c. In particular, we fix two level sets $\mathcal{L}_{I_1}$ and $\mathcal{L}_{I_2}$, and consider a 2-dimensional section of the stable manifold at a small distance $\upsilon = 10^{-5}$ of $\mathcal{L}_{I_2}$, and similarly for the unstable manifold:

$$W^s_\upsilon(\mathcal{L}_{I_2}) := W^s(\mathcal{L}_{I_2}) \cap \{y_1 = \upsilon\}, \tag{4.29}$$

$$W^u_\upsilon(\mathcal{L}_{I_1}) := W^u(\mathcal{L}_{I_1}) \cap \{x_1 = \upsilon\}. \tag{4.30}$$

These sections belong to the boundary of the local stable (resp. unstable) manifolds of Λ_c as given in (4.23).

Integrate the set of initial conditions $W^u_\upsilon(\mathcal{L}_{I_1})$ forwards until they hit the section $\mathcal{S}$, obtaining a set of final points denoted $W^u_\mathcal{S}(\mathcal{L}_{I_1}) \subset \mathcal{S}$. Integrate the set of initial conditions $W^s_\upsilon(\mathcal{L}_{I_2})$ backwards until they hit the section $\mathcal{S}$, obtaining a set of final points denoted $W^s_\mathcal{S}(\mathcal{L}_{I_2}) \subset \mathcal{S}$. Figure 4 shows the sets $W^u_\mathcal{S}(\mathcal{L}_{I_1})$ and $W^s_\mathcal{S}(\mathcal{L}_{I_2})$ for two sample action levels $I_1 = I_2 = 0.12$.

Remark 4.25. We are only considering the 'first' intersection of the stable and unstable manifolds with the section $\mathcal{S}$. We have also explored subsequent (second, third, etc) intersections of the manifolds with the section, but they do not seem to be more interesting for the purpose of diffusion.

For the second step of the procedure, we consider all pairs of points (x_1, x_2) with $x_1 \in W^u_\mathcal{S}(\mathcal{L}_{I_1})$ and $x_2 \in W^s_\mathcal{S}(\mathcal{L}_{I_2})$, and compute the distance $|x_1 - x_2|$. Then we select only those pairs (x_1, x_2) whose distance is below a given threshold, e.g. $|x_1 - x_2| < 0.01$.

Let $y_- \in W^u_\upsilon(\mathcal{L}_{I_1})$ be the initial condition that corresponds to x_1, that is $\Phi^t(y_-) = x_1$. Let $y_+ \in W^s_\upsilon(\mathcal{L}_{I_2})$ be the initial condition that corresponds to x_2, that is $\Phi^{-s}(y_+) = x_2$. Since $|x_1 - x_2|$ is small, the point x_1 is a candidate to homoclinic point, giving rise to an approximate homoclinic orbit from y_- to y_+.

For the third step of the procedure, we use a multidimensional Newton method to refine the initial conditions y_- and y_+ until $|x_1 - x_2| = 0$ within numerical tolerance 10^{-10}. Therefore the point $x = x_1$ is considered a homoclinic point, giving rise to a true homoclinic orbit from y_- to y_+.

For each different homoclinic orbit obtained in the third step, we record the following information:

- initial conditions $y_- \in W^u_\upsilon(\mathcal{L}_{I_1})$ and $y_+ \in W^s_\upsilon(\mathcal{L}_{I_2})$,
- integration times t and s,
- homoclinic point $x \in W^u_\mathcal{S}(\mathcal{L}_{I_1}) \cap W^s_\mathcal{S}(\mathcal{L}_{I_2})$.

Of course, we vary the level sets $\mathcal{L}_{I_1}$ and $\mathcal{L}_{I_2}$ in the range $[0, I_{\max}]$, and repeat the computation procedure explained above to obtain the homoclinic points.

The numerics show that, given two level sets $\mathcal{L}_{I_1}$ and $\mathcal{L}_{I_2}$, typically there are either 8, 4, or 0 homoclinic points. As the value of the level sets changes, one encounters some exceptional values of $\mathcal{L}_{I_1}$ and $\mathcal{L}_{I_2}$ for which the manifolds $W^u_\mathcal{S}(\mathcal{L}_{I_1})$ and $W^s_\mathcal{S}(\mathcal{L}_{I_2})$ intersect tangentially, giving rise to 6 or 2 intersections.

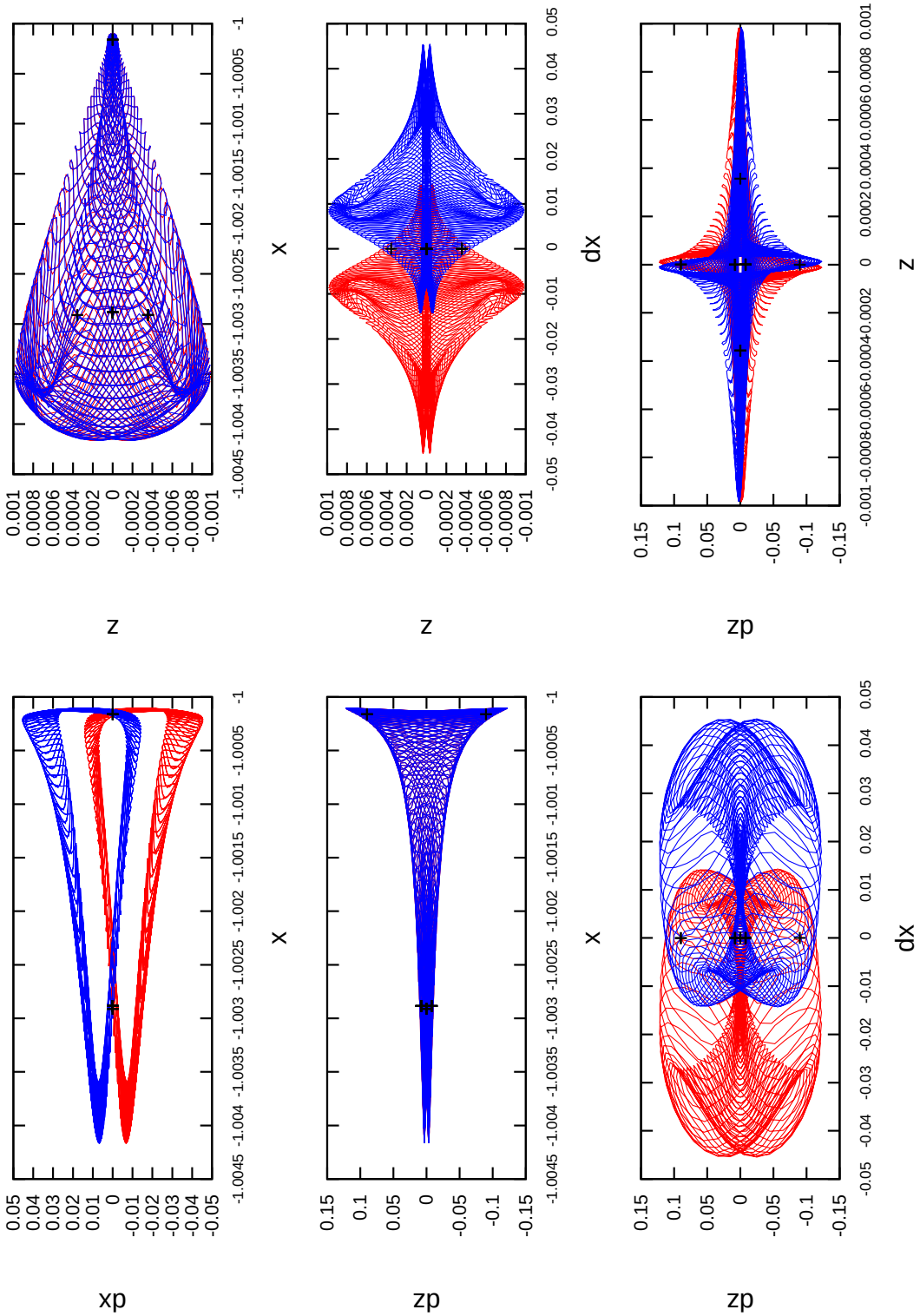

FIGURE 4. Some projections of the set $W^s_S(\mathcal{L}_{\bar{I}})$ (blue) and $W^u_S(\mathcal{L}_{\bar{I}})$ (red) for an sample level set $\mathcal{L}_{\bar{I}}$.

Figure 4 shows the homoclinic points (marked in black) for two sample level sets $I_1 = I_2 = 0.12$. For these particular level sets, there are 8 homoclinic points.

Collecting together all the homoclinic points, we obtain a manifold that corresponds to the the intersection $\Gamma_{\mathcal{S}} := W^s_{\mathcal{S}}(\Lambda_c) \cap W^u_{\mathcal{S}}(\Lambda_c)$. $\Gamma_{\mathcal{S}}$ is precisely the intersection of the stable and unstable manifolds $W^s(\Lambda_c), W^u(\Lambda_c)$ restricted to the section $\mathcal{S}$.

Notice that $\Gamma_{\mathcal{S}}$ is the intersection of two 3-dimensional manifolds $W^s_{\mathcal{S}}(\Lambda_c), W^u_{\mathcal{S}}(\Lambda_c)$ in the 4-dimensional space $M \cap \mathcal{S}$. Thus the intersection $\Gamma_{\mathcal{S}}$ is a 2-dimensional manifold.

4.4. **Computation of scattering maps.** In this section we compute the scattering maps associated to homoclinic manifold found in Section 4.3.

As we shall see, in our model it is difficult to verify what are the maximal homoclinic channels and the corresponding maximally defined scattering maps. However, every triplet of points x, x_-, x_+ satisfying (2.4) and (2.5) locally determine a unique scattering map. The set of points $x-$ (resp. x_+) were these transversality conditions fail is of codimension 1, so they do not appear explicitly in the numerical computation. Also, the numerical verification of the existence of diffusing orbits is based on Theorem 2.4, which assumes the existence of a finite collection of scattering maps, so the fact that do not necessarily distinguish between several scattering maps does not hinder in any way the numerical verification.

The computation of the scattering maps follows easily from the procedure used to compute $W^u(\Lambda_c) \cap W^s(\Lambda_c)$ explained in section 4.3.

Recall that in Section 4.3 that we actually computed $\Gamma_{\mathcal{S}} = W^u_{\mathcal{S}}(\Lambda_c) \cap W^s_{\mathcal{S}}(\Lambda_c)$. Taking the solution curves passing through $\Gamma_{\mathcal{S}}$ yields a homoclinic manifold Γ, whose restriction to the section $\mathcal{S}$ is given by $\Gamma_{\mathcal{S}}$. Notice that the homoclinic manifold Γ is 3-dimensional, while $\Gamma_{\mathcal{S}}$ is 2-dimensional.

Further, recall that the procedure described in Section 4.3 is basically a 'shooting method', where we look for two initial points $y_- \in W^u_\upsilon(\Lambda_c)$ and $y_+ \in W^s_\upsilon(\Lambda_c)$ such that, when integrated forward (resp. backwards) in time up to the section $\mathcal{S}$, they coincide on a single final point $x \in \Gamma_{\mathcal{S}}$. More precisely, we look for the point $x \in \Gamma_{\mathcal{S}}$ by applying a Newton correction to the initial conditions $y_- \in W^u_\upsilon(\Lambda_c)$ and $y_+ \in W^s_\upsilon(\Lambda_c)$ and verifying that

$$\Phi^t(y_-) = \Phi^{-s}(y_+) = x, \tag{4.31}$$

for some integration times $t, s > 0$.

Assume that $x \in W^u(\tilde{x}_-) \cap W^s(\tilde{x}_+)$, where the points $\tilde{x}_-$, $\tilde{x}_+$ are to be determined. Since the fibers $W^u(\tilde{x}_-)$, $W^s(\tilde{x}_+)$ are equivariant under the Hamiltonian flow, $y_- = \Phi^{-t}(x) \in W^u(\Phi^{-t}(\tilde{x}_-))$ and $y_+ = \Phi^s(x) \in W^s(\Phi^s(\tilde{x}_+))$. In fact we have that $y_- \in W^u_\upsilon(\Phi^{-t}(\tilde{x}_-))$, and $y_+ \in W^s_\upsilon(\Phi^s(\tilde{x}_+))$, so, according to (4.27), $y_- = (\tilde{y}_-, \upsilon, 0)$ for some $\tilde{y}_- \in \Lambda_c$ and $y_+ = (\tilde{y}_+, 0, \upsilon)$ for some $\tilde{y}_+ \in \Lambda_c$. Since υ is small, we can approximate $y_- \approx \tilde{y}_-$ and $y_+ \approx \tilde{y}_+$. In other words, the points $\tilde{y}_-$, $\tilde{y}_+$ are obtained from the points y_-, y_+, respectively, by setting both hyperbolic coordinates x_1, y_1 equal to 0. Thus, each of the points $\tilde{y}_-$, $\tilde{y}_+$ is characterized by a set of 3-coordinates of the form (I_v, ϕ_p, ϕ_v). Hence $\Phi^t(\tilde{y}_-) = \tilde{x}_-$ and $\Phi^{-s}(\tilde{y}_+) = \tilde{x}_+$. Thus, $\Omega_-(x) = \tilde{x}_-$ and $\Omega_+(x) = \tilde{x}_+$. We can summarize the computation as follows:

(1) Consider each triplet of points (x, y_-, y_+), with $x \in \Gamma_{\mathcal{S}}$, $y_- = (\tilde{y}_-, \upsilon, 0) \in W^u_\upsilon(\Lambda_c)$ and $y_+ = (\tilde{y}_+, 0, \upsilon) \in W^s_\upsilon(\Lambda_c)$, satisfying (4.31).

(2) Compute $\Phi^t(\tilde{y}_-) = \tilde{x}_-$ and $\Phi^{-s}(\tilde{y}_+) = \tilde{x}_+$, for the precise times t, s that were used in (4.31). We obtain a locally defined scattering map σ associated to the flow Φ^t, given by

$$\tilde{x}_- = \Phi^t(\tilde{y}_-) \xrightarrow{\sigma} \tilde{x}_+ = \Phi^{-s}(\tilde{y}_+).$$

Each scattering map obtained via this algorithm, which is locally defined, can be extended (in a non-unique way) to a maximal domain. At this point we do not attempt to distinguish between different possible scattering maps and find the corresponding maximal domains. Since the points x that we use in this computation are taken from the 2-dimensional manifold $\Gamma_{\mathcal{S}}$, what we obtain are 2-dimensional families of points $\tilde{x}_- \in V_-$, $\tilde{x}_+ \in V_+$ in Λ_c that correspond to one another via locally defined scattering maps σ.

Next we show the result of computing such scattering maps in the SCRTBP. To represent these maps graphically, we show the effect of applying the scattering maps to several action level sets of the normalized action $I = I_v/I_{max}$ (the maximal value of the normalized action being equal to 1). The results are shown in Figure 5.

Let us clarify a few things about Figure 5:

- Each σ is π-periodic in the out-of-plane angle ϕ_v. This is due to the $z = 0$ symmetry in the SCRTBP.
- For each normalized action value $I = 0.005, 0.010, 0.015, 0.020$, we identify a set V_-, contained in the action level set, which consists of two non-contractible red curves on the torus and are homeomorphic to a circle S^1. The corresponding set $V+$ consists of two 'sinusoidal-like' blue curves. The 'leftmost' red curve (consisting of points with $\phi_p < \pi$) is mapped to the leftmost blue curve, while the 'rightmost' red curve (consisting of points with $\phi_p > \pi$) is mapped to the rightmost blue curve.
- For each action value $I_v = 0.025, 0.030$, we identify a set V_-, contained in the action level set, which consists of two red curves contractible to a point on the torus. The corresponding set $V+$ consists of two blue 'figure-eight-like' closed loops. They do not look like closed loops, because $\phi_p = 0$ and $\phi_p = 2\pi$ need to be identified. However when we identify both sides, we do indeed see two closed loops. The 'center' red curve (consisting of points with $2 < \phi_v < 5$) is mapped to the center blue loop, while the 'displaced' red curve (consisting of points with $\phi_v < 2$ or $\phi_v > 5$) is mapped to the displaced blue loop.
- Based on the numerical evidence, there seem to be (at least) two scattering maps whose domains are disjoint open sets in Λ_c, and whose intersections with $I = $ const. contain the two components of the set V_-. As mentioned before, it is non straightforward to precisely identify the homoclinic channels within the homoclinic manifold, and the corresponding scattering maps, and also to identify the maximal domains of these scattering map. The point is that, in order to establish the existence of diffusing trajectories, distinguishing between different scattering maps is not relevant for the argument.
- The curves depicted in Figure 5, despite some apparent gaps, are in fact continuous. These visible gaps are due to the discrete nature of our numerics. Of course, using more action-level sets and more points on those

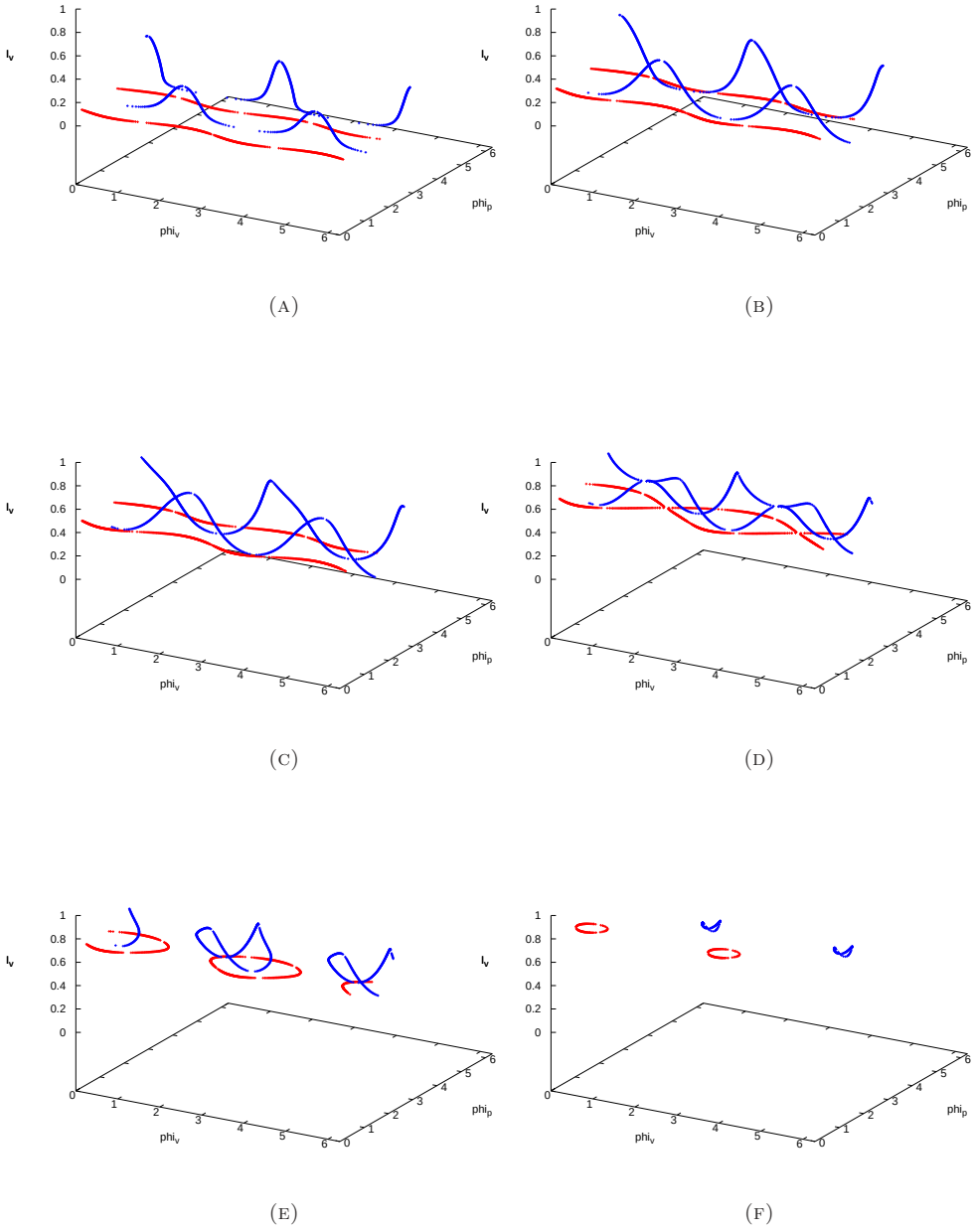

(A) (B)

(C) (D)

(E) (F)

FIGURE 5. Effect of the scattering map on the normalized action level sets $I = 0.12, 0.29, 0.47, 0.65, 0.71, 0.82$ (left to right and top to bottom). Each plot shows an action level set (red) and its image under the scattering map (blue). See text for more details.

level sets would give a better approximation of the scattering maps, filling in those gaps.

Next, we compute scattering maps σ^Σ associated to the first return map F to the surface of section Σ in Λ_c, as in 2.3.

We transport each point $\tilde{x}_-$, $\tilde{x}_+$ in Λ_c by the flow Φ^t until the in-plane angle ϕ_p becomes 0. We set $x_- = \Phi^{\tau(\tilde{x}_-)}(\tilde{x}_-)$ and $x_+ = \Phi^{\tau(\tilde{x}_+)}(\tilde{x}_+)$, where $\tau(\tilde{x}_\pm)$ is the first instant of time when the flow trajectory $\Phi^t(\tilde{x}_\pm)$ intersects Σ.

We obtain numerically computed scattering maps σ^Σ associated to the first return map F to Σ, given by

$$x_- = \Phi^{\tau(\tilde{x}_-)}(\tilde{x}_-) \xrightarrow{\sigma^\Sigma} x_+ = \Phi^{\tau(\tilde{x}_+)}(\tilde{x}_+).$$

Each point x_-, x_+ is described by a pair of coordinates of the form (I_v, ϕ_v). Since (I_v, ϕ_v) are our distinguished coordinates, from now on we will denote them $(I, \phi) := (I_v, \phi_v)$ for simplicity. We let $x_- = (I_-, \phi_-)$ and $x_+ = (I_+, \phi_+)$.

The results of computing the scattering maps reduced to the surface of section Σ are shown in figure 6. We show the effect of applying the scattering maps to several action level sets. An action level set here is a set of points in Σ with fixed action $I = \bar{I}$, i.e. lying on a horizontal line in the (I, ϕ)-plane.

Let us clarify some things about figure 6:

- We have selected a scattering map σ^Σ corresponding to one of the two numerically identified scattering maps σ for the flow. More precisely, we have selected the scattering map σ that has the maximum effect on action level sets.
- Again, we do not identify the maximal domain of the scattering map σ^Σ, so we may in fact have several scattering maps σ^Σ rather than a single one. However, we stress again that main theoretical result Theorem 2.4 is valid even when one deals with several scattering maps, so we do not necessarily need to make distinction between various scattering maps.
- In addition to action level sets and their images by the scattering map σ^Σ, we also depict some (rectangle-like) topological disks and their images by the scattering map, i.e., $1 \xrightarrow{\sigma^\Sigma} 2$, $3 \xrightarrow{\sigma^\Sigma} 4$, $5 \xrightarrow{\sigma^\Sigma} 6$. The color code suggests that, besides the effect on the action level sets, the scattering map also has a twist effect, as it tilts vertical lines to the right. The topological disks are chosen so that the image of 2 under some power of F contains 3 in its interior, and the image 4 under some power of F contains 5 in its interior. More details are given in Section 4.5. The color code shows that F is also a twist map in the reverse direction, as it tilts vertical lines to the left.

We now compare the effect of scattering map σ^Σ on action level sets for different energy levels. In figure 7 we have a schematic representation on the effect of scattering map on action level sets for $c = 3.00087$ — closer to $c_1 = C(L_1)$ —, and for $c = 3.00083$ — closer to $c_{halo} = C(halo)$. A marked dot in each of these diagrams signifies the possibility to move with a scattering map from an action level set corresponding to normalized value of action equal to the horizontal coordinate of the dot, to a an action level set corresponding to a normalized value of action equal to the vertical coordinate of the dot. A normalized value of the action equal to 1 corresponds to $I_v = I_{max}$, the largest possible value of the action coordinate for the corresponding energy level. We remark that the closer c is to $C(L_1)$, the

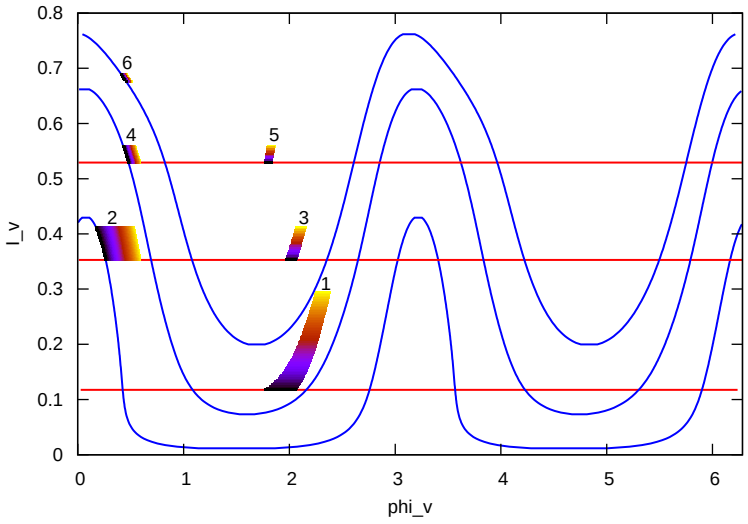

FIGURE 6. Two-dimensional projection of three different level sets of the normalized action (red lines) and of their images by the scattering maps (blue lines). Locally, the scattering map is continued to rectangle-like sets. Rectangle 1 is mapped by the scattering map onto rectangle 2, rectangle 3 is mapped by the scattering map onto rectangle 4, and rectangle 5 is mapped by the scattering map onto rectangle 6.

smaller is the normalized action that can be reached via this mechanism, and the the closer c is to $C(halo)$, the larger is normalized action that that can be reached via this mechanism.

Remark 4.26. We also note that numerical computation of the scattering map, similar to this one, in different models from celestial mechanics, have been performed in [6, 22]. A related concept to that of scattering map that is more closely associated to trajectories in the phase space is that of the transition map, introduced in [17]; with the notation from above, a transition map is given by the map $y_- \mapsto y_+$.

4.5. **Existence of diffusing orbits.** We first summarize the geometric structures that have been identified numerically so far, and explain how to apply Theorem 2.6 to show the existence of diffusing orbits.

Our numerical procedure produced the following geometric objects:

- For some fixed levels of the Jacobi constant $c \in [c_{halo} + \epsilon_0, c_1)$ we have obtained numerical approximations of the NHIM $\Lambda_c \simeq S^3$, via the Birkhoff normal form procedure in Section 4.1.1. Each such NHIM is parametrized by a system of coordinates (I_v, ϕ_p, ϕ_v). (We recall that in our theoretical argument we assumed that the normally hyperbolic invariant manifold Λ_c

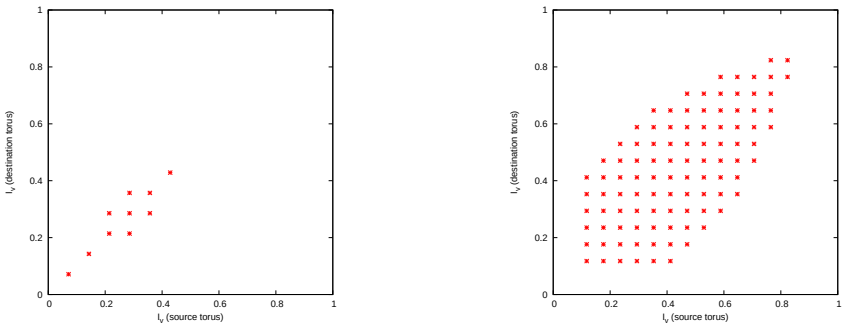

FIGURE 7. Effect of scattering map on action level sets for different energy levels for $c = 3.00087$ (left) and $c = 3.00083$ (right). Both axes are labeled by values of the normalized action.

exists, is uniquely defined, and is diffeomorphic to S^3, for each c in this energy range.)

- We have identified numerically the transverse intersection of the manifolds $W^u(\Lambda_c)$, $W^s(\Lambda_c)$ within the surface of section $\mathcal{S} = \{y = 0, \dot{y} > 0\}$, consisting of homoclinic orbits that execute 1-turn around the Earth. Corresponding to this transverse homoclinic intersections we have computed numerically and identified two scattering maps, that have different effects on action level sets. These scattering maps take values on Λ_c. We have selected and fixed the scattering map σ that has the largest effect on action level sets. (As we did not compute the corresponding homoclinic channels, each of the numerically identified scattering maps may in fact be the juxtaposition of several scattering maps defined on maximal domains.)
- In Λ_c we have built a finite grid of $I := I_v$-action level sets such that the unstable manifold of each action level set intersects the stable manifolds of one or more of the neighboring level sets in the grid. (We recall that these level sets are not invariant under the Hamiltonian flow.)
- We have fixed a local surface of section $\Sigma = \{\phi_2 = 0, \dot{\phi}_2 > 0\}$ in a neighborhood of Λ_c and computed the first return map F to Σ. The manifold $\Lambda_c^\Sigma = \Lambda_c \cap \Sigma$ is a NHIM for F. The selected scattering map σ for the Hamiltonian map induces a scattering map corresponding to the return map. We have identified a finite sequence of level sets $\mathcal{L}^\Sigma_{I_0}, \ldots, \mathcal{L}^\Sigma_{I_N}$ in Λ_c^Σ, such that for each $j = 0, \ldots, N-1$, $\sigma^\Sigma(\mathcal{L}^\Sigma_{I_j})$ intersects transversally $\mathcal{L}^\Sigma_{I_{j+1}}$.
- We construct a sequence of topological disks B_j in Λ_c^Σ, $j = 0, \ldots, N-1$, such that:
  - each B_j is contained in a neighborhood of diameter δ_j of some point $(I_j, \phi_j) \in \mathcal{L}^\Sigma_{I_j}$, for some suitable $\delta_j > 0$, and
  - for each $j = 0, \ldots, N-1$, $\text{int}[F^{k_j} \circ \sigma^\Sigma(B_j)] \supseteq B_{j+1}$, for some $k_j > 0$.
- Choosing $\delta > \max_j \delta_j$, Theorem 2.6 implies the existence of a trajectory $\Phi^t(z)$ of the Hamiltonian flow and of times t_j such that $d(\Phi^{t_j}(z), \mathcal{L}_{I_j}) < \delta$, for $j = 0, \ldots, N-1$.

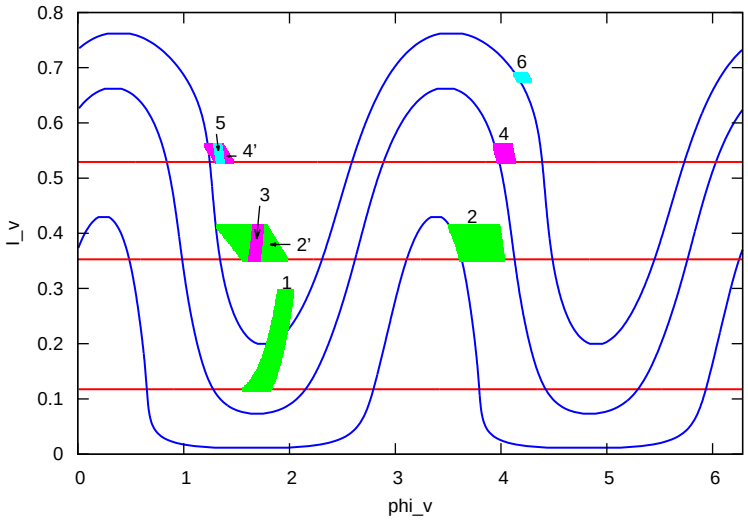

FIGURE 8. Two-dimensional scattering map acting on three different level sets of the normalized action (red lines). The topological disk 1 is mapped to 2 by the scattering map. The topological disk 2 is mapped to 2' after 11 iterations. The topological disk 2' contains 3 in its interior. The topological disk 3 is mapped to 4 by the scattering map. The topological disk 4 is mapped to 4' after 12 iterations. The topological disk 4' contains 5 in its interior. The topological disk 5 is mapped to 6 by the scattering map.

The numerical construction of the topological disks is shown in Figure 8. First we identify four action level sets $\mathcal{L}^{\Sigma}_{I_0} = 0.12$, $\mathcal{L}^{\Sigma}_{I_1} = 0.35$, $\mathcal{L}^{\Sigma}_{I_2} = 0.53$, and $\mathcal{L}^{\Sigma}_{I_3} = 0.71$ such that $\sigma^{\Sigma}(\mathcal{L}^{\Sigma}_{I_j})$ intersects transversally $\mathcal{L}^{\Sigma}_{I_{j+1}}$, for $j = 0, 1, 2$. The first three level sets are shown in red. Their image by the scattering map is shown in blue. The last level set is not shown in the figure.

Then we choose a sequence of points $(I_j, \phi_j) \in \mathcal{L}^{\Sigma}_{I_j}$ such that each of these points is mapped by the scattering map to the next action level set: $\sigma^{\Sigma}(I_j, \phi_j) \in \mathcal{L}^{\Sigma}_{I_{j+1}}$ for $j = 0, 1, 2$. In the picture, the first point (I_0, ϕ_0) is located on the topological disk 1, the second point (I_1, ϕ_1) is on disk 3, and the third point (I_2, ϕ_2) is on disk 5. These points are actually not shown in the figure to avoid cluttering. Their respective images are located on disks 2, 4, and 6.

Then we construct a sequence of topological disks (denoted 1 to 5 in the figure) in Λ_{Σ} such that:

- disc 1 is mapped to disc 2 by the scattering map σ^{Σ}, disc 3 to disc 4, and disc 5 to disc 6.

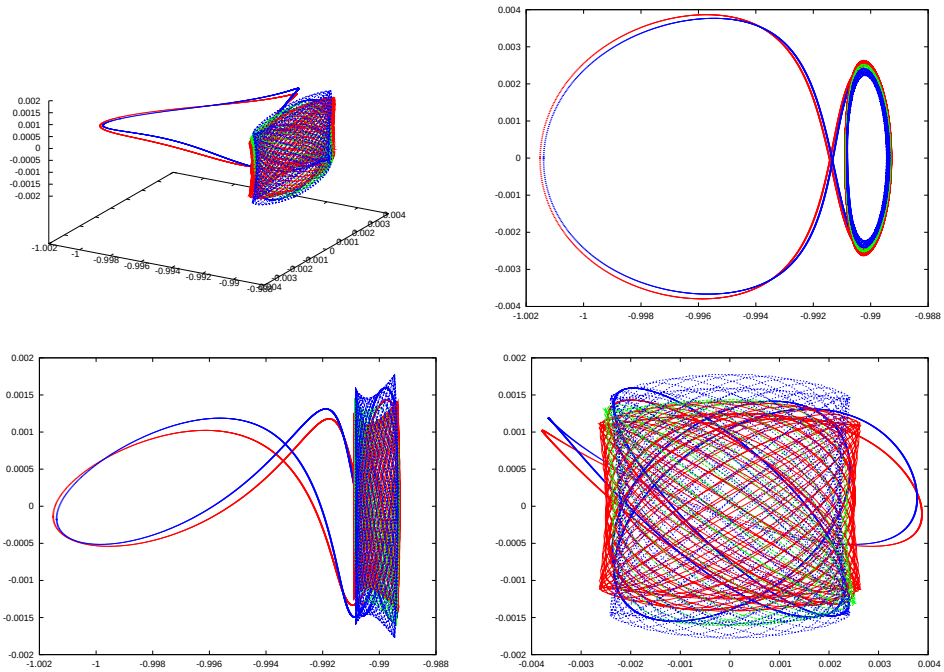

FIGURE 9. An example of a diffusing orbit, in four different projections.

- disc 2 is mapped by the first return map F to disc 2' after 11 iterations, and disc 4 is mapped by F to disc 4' after 12 iterations.
- disc 3 is contained strictly inside disc 2', and disc 5 is contained strictly inside disc 4'.
- the diameter of the discs are: disc 1: $\delta_0 = 0.18$, disc 3: $\delta_1 = 0.06$, disc 5: $\delta_2 = 0.01$.

Therefore, choosing $\delta > 0.18$, Theorem 2.6 implies the existence of a trajectory $\Phi^t(z)$ of the Hamiltonian flow and of times t_j such that $d(\Phi^{t_j}(z), \mathcal{L}_{I_j}) < \delta$, for $j = 0, 1, 2$.

An example of a diffusing trajectory obtained via this mechanism is shown in figure 9.

ACKNOWLEDGEMENT

Part of this work has been done while M.G. was visiting the Centre de Recerca Matemàtica, Barcelona, Spain, for whose hospitality he is very grateful.

REFERENCES

[1] V.I. Arnold. Instability of dynamical systems with several degrees of freedom. *Sov. Math. Doklady*, 5:581–585, 1964.

[2] P. Bernard, V. Kaloshin, and K. Zhang. Arnold diffusion in arbitrary degrees of freedom and 3-dimensional normally hyperbolic invariant cylinders, arXiv:1112.2773.

[3] U. Bessi. An approach to arnol'd's diffusion through the calculus of variations. *Nonlinear Anal.*, 26:1115–1135, 1996.

[4] S. Bolotin and D. Treschev. Unbounded growth of energy in nonautonomous Hamiltonian systems. *Nonlinearity*, 12(2):365–388, 1999.
[5] Sławomir Breiter. *Dynamics and Astrometry of Natural and Artificial Celestial Bodies: Proceedings of IAU Colloquium 165 Poznań, Poland July 1 – 5, 1996*, chapter Semi-Analytical and Semi-Numerical Methods in Celestial Mechanics, pages 411–418. Springer Netherlands, Dordrecht, 1997.
[6] E. Canalias, A. Delshams, J. J. Masdemont, and P. Roldán. The scattering map in the planar restricted three body problem. *Celestial Mech. Dynam. Astronom.*, 95(1-4):155–171, 2006.
[7] M. Capinski, M. Gidea, and R. De la Llave. Arnold diffusion in the planar elliptic restricted three-body problem: mechanism and numerical simulation, 2014.
[8] Maciej J. Capiński and Pablo Roldán. Existence of a center manifold in a practical domain around L_1 in the restricted three-body problem. *SIAM J. Appl. Dyn. Syst.*, 11(1):285–318, 2012.
[9] Maciej J. Capiński and Piotr Zgliczyński. Transition tori in the planar restricted elliptic three body problem, preprint. *Nonlinearity*, 24(5):1395, 2011.
[10] C.-Q. Cheng. Arnold diffusion in nearly integrable Hamiltonian systems. *ArXiv e-prints*, July 2012.
[11] Chong-Qing Cheng and Jun Yan. Existence of diffusion orbits in a priori unstable Hamiltonian systems. *J. Differential Geom.*, 67(3):457–517, 2004.
[12] Chong-Qing Cheng and Jun Yan. Arnold diffusion in Hamiltonian systems: a priori unstable case. *J. Differential Geom.*, 82(2):229–277, 2009.
[13] L. Chierchia and G. Gallavotti. Drift and diffusion in phase space. *Ann. Inst. H. Poincaré Phys. Théor.*, 60(1):144, 1994.
[14] George Contopoulos. *Order and chaos in dynamical astronomy*. Astronomy and Astrophysics Library. Springer-Verlag, Berlin, 2002.
[15] Rafael de la Llave. Orbits of unbounded energy in perturbations of geodesic flows by periodic potentials. a simple construction. Preprint, 2004.
[16] A. Delshams, R. de la Llave, and T. M-Seara. A geometric mechanism for diffusion in Hamiltonian systems overcoming the large gap problem: heuristics and rigorous verification on a model. *Mem. Amer. Math. Soc.*, 179(844):viii+141, 2006.
[17] A. Delshams, M. Gidea, and P. Roldan. Transition map and shadowing lemma for normally hyperbolic invariant manifolds. *Discrete and Continuous Dynamical Systems. Series A.*, 3(33):1089–1112, 2013.
[18] Amadeu Delshams, Rafael de la Llave, and Tere M. Seara. A geometric approach to the existence of orbits with unbounded energy in generic periodic perturbations by a potential of generic geodesic flows of $\mathbf{T}^2$. *Comm. Math. Phys.*, 209(2):353–392, 2000.
[19] Amadeu Delshams, Rafael de la Llave, and Tere M. Seara. A geometric mechanism for diffusion in Hamiltonian systems overcoming the large gap problem: announcement of results. *Electron. Res. Announc. Amer. Math. Soc.*, 9:125–134, 2003.
[20] Amadeu Delshams, Rafael de la Llave, and Tere M. Seara. Orbits of unbounded energy in quasi-periodic perturbations of geodesic flows. *Adv. Math.*, 202(1):64–188, 2006.
[21] Amadeu Delshams, Rafael de la Llave, and Tere M. Seara. Geometric properties of the scattering map of a normally hyperbolic invariant manifold. *Adv. Math.*, 217(3):1096–1153, 2008.
[22] Amadeu Delshams, Josep Masdemont, and Pablo Roldán. Computing the scattering map in the spatial Hill's problem. *Discrete Contin. Dyn. Syst. Ser. B*, 10(2-3):455–483, 2008.
[23] Jagiellonian University Division of Computational Mathematics. CAPD – computer assisted proofs in dynamics. `http://capd.ii.uj.edu.pl/`.
[24] J. Fejoz, M. Guardia, V. Kaloshin, and P. Roldan. Kirkwood gaps and diffusion along mean motion resonance for the restricted planar three body problem. *Journal of the European Mathematical Society*, 2013.
[25] N. Fenichel. Asymptotic stability with rate conditions. *Indiana Univ. Math. J.*, 23:1109–1137, 1973/74.
[26] E. Fontich and P. Martín. Differentiable invariant manifolds for partially hyperbolic tori and a lambda lemma. *Nonlinearity*, 13(5):1561–1593, 2000.
[27] E. Fontich and P. Martín. Arnold diffusion in perturbations of analytic integrable Hamiltonian systems. *Disc. Cont. Dyn. Syst.*, 7(1):61–84, 2001.
[28] J. Galante and V. Kaloshin. Destruction of invariant curves using comparison of action, preprint, 2011.

[29] J. Galante and V. Kaloshin. The method of spreading cumulative twist and its application to the restricted circular planar three body problem, preprint, 2011.
[30] Vassili Gelfreich and Dmitry Turaev. Unbounded energy growth in Hamiltonian systems with a slowly varying parameter. *Comm. Math. Phys.*, 283(3):769–794, 2008.
[31] M. Gidea and C. Robinson. Diffusion along transition chains of invariant tori and aubry-mather sets. *Ergodic Theory Dynam. Systems*, 33:1401–1449, 2013.
[32] Marian Gidea and Rafael de la Llave. Topological methods in the instability problem of Hamiltonian systems. *Discrete Contin. Dyn. Syst.*, 14(2):295–328, 2006.
[33] Marian Gidea, Rafael de la Llave, and Tere Seara. A general mechanism of diffusion in hamiltonian systems: Qualitative results, 2014.
[34] G. Gómez, À. Jorba, C. Simó, and J. Masdemont. *Dynamics and mission design near libration points. Vol. III*, volume 4 of *World Scientific Monograph Series in Mathematics*. World Scientific Publishing Co. Inc., River Edge, NJ, 2001. Advanced methods for collinear points.
[35] G. Gómez, W. S. Koon, M. W. Lo, J. E. Marsden, J. Masdemont, and S. D. Ross. Connecting orbits and invariant manifolds in the spatial restricted three-body problem. *Nonlinearity*, 17(5):1571–1606, 2004.
[36] G. Gómez, J. Masdemont, and C. Simó. Lissajous orbits around halo orbits, 1997.
[37] Àngel Jorba. A methodology for the numerical computation of normal forms, centre manifolds and first integrals of Hamiltonian systems. *Experiment. Math.*, 8(2):155–195, 1999.
[38] Àngel Jorba and Josep Masdemont. Dynamics in the center manifold of the collinear points of the restricted three body problem. *Phys. D*, 132(1-2):189–213, 1999.
[39] V. Kaloshin. Geometric proofs of Mather's connecting and accelerating theorems. In *Topics in dynamics and ergodic theory*, volume 310 of *London Math. Soc. Lecture Note Ser.*, pages 81–106. Cambridge Univ. Press, Cambridge, 2003.
[40] V. Kaloshin and K. Zhang. Normally hyperbolic invariant manifolds near strong double resonance, arXiv:1202.1032.
[41] V. Kaloshin and K. Zhang. A strong form of arnold diffusion for two and a half degrees of freedom, arXiv:1212.1150.
[42] Jaume Llibre, Regina Martínez, and Carles Simó. Tranversality of the invariant manifolds associated to the Lyapunov family of periodic orbits near L_2 in the restricted three-body problem. *J. Differential Equations*, 58(1):104–156, 1985.
[43] P. Lochak, J.-P. Marco, and D. Sauzin. On the splitting of invariant manifolds in multidimensional near-integrable Hamiltonian systems. *Mem. Amer. Math. Soc.*, 163(775):viii+145, 2003.
[44] J. J. Masdemont. High-order expansions of invariant manifolds of libration point orbits with applications to mission design. *Dyn. Syst.*, 20(1):59–113, 2005.
[45] John N. Mather. Arnol′d diffusion. I. Announcement of results. *J. Math. Sci. (N. Y.)*, 124(5):5275–5289, 2004.
[46] John N. Mather. Arnold diffusion by variational methods. In *Essays in mathematics and its applications*, pages 271–285. Springer, Heidelberg, 2012.
[47] Kenneth R. Meyer, Glen R. Hall, and Dan Offin. *Introduction to Hamiltonian dynamical systems and the N-body problem*, volume 90 of *Applied Mathematical Sciences*. Springer, New York, second edition, 2009.
[48] Richard Moeckel. Transition tori in the five-body problem. *J. Differential Equations*, 129(2):290–314, 1996.
[49] Richard Moeckel. Isolating blocks near the collinear relative equilibria of the three-body problem. *Trans. Amer. Math. Soc.*, 356(11):4395–4425 (electronic), 2004.
[50] James Murdock. *Normal forms and unfoldings for local dynamical systems*. Springer Monographs in Mathematics. Springer-Verlag, New York, 2003.
[51] G. N. Piftankin. Diffusion speed in the Mather problem. *Dokl. Akad. Nauk*, 408(6):736–737, 2006.
[52] Charles Pugh and Michael Shub. Linearization of normally hyperbolic diffeomorphisms and flows. *Invent. Math.*, 10:187–198, 1970.
[53] David L. Richardson. A note on a Lagrangian formulation for motion about the collinear points. *Celestial Mech.*, 22(3):231–236, 1980.
[54] C. Robinson. Symbolic dynamics for transition tori. *Contemporary Math.*, 292:199–208, 2002.
[55] P. Robutel and F. Gabern. The resonant structure of jupiters trojan asteroids i: Long term stability and diffusion. *Mon. Not. R. Astron. Soc., 122 (2006)*, 000:1–22, 2006.

[56] A. Samà-Camí. Equilibria in three body problems: stability, invariant tori and connections. phd thesis, Universitat Autònoma de Barcelona. 2004.
[57] Jan Sijbrand. Properties of center manifolds. *Transactions of the American Mathematical Society*, 289(2):431–469, 1985.
[58] V. Szebehely. *Theory of Orbits*. Academic Press, 1967.
[59] D. Treschev. Evolution of slow variables in a priori unstable Hamiltonian systems. *Nonlinearity*, 17(5):1803–1841, 2004.
[60] Zhihong Xia. Arnol′d diffusion in the elliptic restricted three-body problem. *J. Dynam. Differential Equations*, 5(2):219–240, 1993.
[61] Zhihong Xia. Arnol′d diffusion and oscillatory solutions in the planar three-body problem. *J. Differential Equations*, 110(2):289–321, 1994.
[62] Jinxin Xue. Arnold diffusion in a restricted planar four-body problem. *Nonlinearity*, 27(12):2887, 2014.

Departament de Matemática Aplicada I, ETSEIB-UPC, 08028 Barcelona, Spain
E-mail address: Amadeu.Delshams@upc.edu

School of Civil Engineering and Architecture, Xiamen University of Technology, Fujian, China, and Department of Mathematical Sciences, Yeshiva University, New York, NY 10018, USA
E-mail address: Marian.Gidea@yu.edu

Departamento de Matemáticas, Instituto Tecnológico Autónomo de México, CDMX 01080, México
E-mail address: Pablo.Roldan@itam.mx